Supplementary Material for

Hypoxia-Inducible Factor 1α Stabilization Restores Epigenetic Control of Nitric Oxide Synthase 1 Expression and Reverses Gastroparesis in Female Diabetic Mice

Fei Gao, Yujiro Hayashi, Siva Arumugam Saravanaperumal, Gabriella B. Gajdos, Sabriya A. Syed, Aditya V. Bhagwate, Zhenqing Ye, Jian Zhong, Yuebo Zhang, Egan L. Choi, Sergiy M. Kvasha, Jagneet Kaur, Brooke D. Paradise, Liang Cheng, Brandon W. Simone, Alec M. Wright, Todd A. Kellogg, Michael L. Kendrick, Travis J. McKenzie, Zhifu Sun, Huihuang Yan, Chuanhe Yu, Adil E. Bharucha, David R. Linden, Jeong-Heon Lee, and Tamas Ordog

Contents:

Supplementary Methods

Regulatory Approvals

De-identified gastric tissues were collected from 6 female nondiabetic (33, 34, 38, 45, 47 and 52 years of age) and 9 female diabetic (30, 36, 36, 40, 41, 42, 47, 48, and 54 years of age) patients undergoing bariatric surgery with the approval of the Mayo Clinic Institutional Review Board (IRB 13-008138). Oral consent was obtained by the surgical teams before the surgery and recorded in the patients' electronic medical record. In addition, gastric tissues from bariatric surgeries were also obtained from 1 female nondiabetic patient (41 years of age), 3 male nondiabetic patients (28, 49, and 67 years of age), and 2 female diabetic patients (36 and 59 years of age) through a clinical research project (IRB 20-012002). These patients also underwent bariatric surgeries after providing written consent.

The animal care and use program and facilities at Mayo Clinic meet all federal regulations and guidelines. Mayo Clinic is registered with the USDA (41-R-0006) as an animal research facility and maintains a National Institutes of Health animal assurance statement (A3291-01) with the Office of Laboratory Animal Welfare. Mayo Clinic's animal care and use programs and facilities have been reviewed and are fully accredited by the Association for Assessment and Accreditation of Laboratory Animal Care International (AAALAC). Animal experiments were performed in accordance with the National Institutes of Health Guide for the Care and Use of Laboratory Animals and ARRIVE guidelines. The protocols were approved by the Mayo Clinic Institutional Animal Care and Use Committee (A48315-15 and A2508-08).

Protocols for work with biohazardous agents, recombinant DNA, and synthetic nucleic acids including plasmids, lentivectors, and small interfering RNA were approved by the Mayo Clinic Institutional Biosafety Committee (Bios00000076.01). Work with these agents was performed at biocontainment level BSL2 or BSL2+ according to standard operating procedures covering personal protective equipment use, decontamination and waste handling.

Materials

Pimonidazole HCl was purchased as a component of the Hypoxyprobe-Red594 Kit from Hypoxyprobe, Inc. (Burlington, MA). 4',6-diamidino-2-phenylindole (DAPI) was purchased from Thermo Fisher Scientific, Waltham, MA. MG132 was from Calbiochem (EMD Millipore, Billerica, MA). FG-4592 was from Cayman Chemical (Ann Arbor, MI) or Selleck Chemical (Houston, TX). Tamoxifen, peanut oil, dimethyl sulfoxide (DMSO), and Triton-X were from Sigma-Aldrich (St. Louis, MO). Alexa Fluor 647 (AF647)-labeled cholera toxin subunit B (CTB-AF647) was purchased from Thermo Fisher Scientific.

Human Tissues

Full thickness gastric corpus tissues representing most of the greater curvature of the stomach were obtained from gastric bypass surgeries (gastric sleeve procedure) for obesity. This surgery involves removal of part of the stomach which is surgical waste tissue. The tissues were placed into ice-cold F12 medium (Thermo Fisher Scientific) and immediately transported to the lab for fixation. Pieces of the tunica muscularis were prepared by cutting away the mucosa and submucosa.

Animal Models, Housing, and Husbandry

Mapt$^{tm1(EGFP)Klt}$/J mice (*Mapt*-EGFP; The Jackson Laboratory, Bar Harbor, ME; stock 004779) carry a knock-in of the *EGFP* (enhanced green fluorescent protein) coding sequence in the first exon of the microtubule-associated protein tau (*Mapt*) gene producing a cytoplasmic EGFP fused to the first 31 amino acids of MAPT. EGFP expression marks neurons including enteric neurons regardless of their lineage, closely patterning the expression of neuron-specific beta-tubulin III (TUBB3). These mice are viable, fertile, normal in size and do not display any gross physical or behavioral abnormalities.[1] The mice were backcrossed to C57BL/6J (The Jackson Laboratory; stock 000664) for three to five generations at Mayo Clinic. The strain was then maintained by homozygous breeding.

B6.129-*Nos1*$^{tm1(cre)Mgmj}$/J mice (*Nos1*^{cre}; The Jackson Laboratory; stock 017526) express Cre recombinase from the 3' untranslated region (UTR) of the endogenous *Nos1* locus. Mice homozygous for the targeted mutation are viable and fertile.[2] Recently, germline recombination in the F2 generation of Cre;floxed double mutant female (F1) *Nos1*^{cre} mice bred to floxed and/or wildtype mice has been reported.[3,4] In our hands, recombination in the gut of the F2 generation occurred in non-nitrergic neurons and other cell types rather broadly but to a variable degree, possibly due to germline recombination[4].

B6;129S-*Nos1*$^{tm1.1(cre/ERT2)Zjh}$/J mice (*Nos1*$^{creERT2/+}$; The Jackson Laboratory; stock 014541) possess a knock-in allele that abolishes *Nos1* gene function and expresses CreERT2 fusion protein from the *Nos1* promoter/enhancer elements. Heterozygous mice of this strain are viable, fertile, normal in size and do not display any gross physical or behavioral abnormalities.[5]

Mice expressing switchable, membrane- or nucleus-targeted tandem dimer Tomato-EGFP reporter constructs (*Gt(ROSA)26Sor*$^{tm4(ACTB-tdTomato,-EGFP)Luo}$/J[6] (*R26*^{mTmG}; The Jackson Laboratory; stock 007576) and B6;129S6-*Gt(ROSA)26Sor*$^{tm1(CAG-tdTomato*,-EGFP*)Ees}$/J (*R26*^{nTnG}; The Jackson Laboratory; stock 023035), respectively) were used as reporters of *Nos1* expression. Both strains were maintained by homozygous breeding.

B6.129-*Hif1a*^{tm3Rsjo}/J mice (*Hif1a*^{fl}; The Jackson Laboratory; stock 007561) have *loxP* sites flanking exon 2 of *Hif1a*. Exposure to Cre recombinase creates a null allele. This strain was also maintained by homozygous breeding.

C57BL/6J mice were from The Jackson Laboratory (stock 000664).

Gt(ROSA)26Sor$^{tm1(DTA)Jpmb}$/J mice (*R26*$^{LSL(EGFP)-DTA}$; The Jackson Laboratory; stock 006331), which have a *loxP*-flanked STOP sequence (*EGFP*::PGK-neo::3xpolyA) upstream of the diphtheria toxin A subunit (DTA) gene, preventing its transcription, show widespread expression of EGFP. Homozygous mice of this strain were used as compensation and positive controls in FACS experiments utilizing EGFP as a fluorescent reporter.

Except for the in vivo gastric emptying and gastric volume studies, which were performed in female streptozotocin-diabetic C57BL/6J mice, both male and female animals were used. None of the mice were used in any previous experiments.

Mice were housed maximum 5/cage using an Allentown, Inc. (Allentown, NJ) reusable static caging system in the Mayo Clinic Department of Comparative Medicine Guggenheim Vivarium under a 12 h light/12 h dark cycle observing environmental enrichment and social housing

guidelines. Bedding material was irradiated one-quarter inch corn cob with the addition of Bed-r'Nest irradiated paper-twist nesting material (4 g), Twist-n'Rich (8") (The Andersons, Inc., Maumee, OH), and Safe Harbor Mouse Retreat (K3583, Bio-Serv, Flemington, NJ) as enrichment. Mice were kept on irradiated PicoLab® 5058 Mouse Diet 20 (≥20% protein, ≥9% fat, ≤4% fiber, ≤6.5% ash, ≤12% moisture; LabDiet, Inc., St. Louis, MO). Food and water were available ad libitum. Before GE and GV studies, mice were fasted overnight in a metabolic cage with free access to water. Animals were handled during the light phase.

In Vivo Animal Experiments

Labeling of intestinofugal neurons. Six male and six female *Mapt*-EGFP mice (54-98 days of age) underwent surgical laparotomy in 3 groups (surgery #1: 1 male and 1 female, surgery #2: 3 males and 1 female, surgery #3: 2 males and 4 females) under pentobarbital (50mg/kg) anesthesia. The celiac ganglion of each mouse was injected with 3-5 µL of 25 mg/mL CTB-AF647 with the intention of labeling the cell soma of intestinofugal neurons in the myenteric plexus of the colon. The animals were euthanized 3-4 days after surgery.

Labeling of hypoxic cells in vivo. Mice were injected with 60mg/kg (2.4 mg/40 µl phosphate-buffered saline) Pimonidazole HCl (Hypoxyprobe, Inc) intraperitoneally 60 minutes prior to euthanasia.[7,8] Control mice were injected with vehicle.

Induction of Cre-mediated recombination in vivo. Cre-mediated recombination was induced with tamoxifen (Sigma-Aldrich) injected intraperitoneally once daily for 3 or 5 consecutive days at a dose of 0.075 mg/g body weight in peanut oil vehicle (Sigma Aldrich) containing 10% ethanol (3.75 µL/g body weight). Control animals were injected with peanut oil vehicle. Animals were euthanized at least 6 days after the initiation of the tamoxifen treatment.

Induction of diabetes using streptozotocin. Previously published methods were used.[9] Female C57BL/6J mice weighing more than 20 g (9-10 weeks of age) were starved for 4 h prior to streptozotocin injection. Freshly prepared streptozotocin (20 mg/mL in 50 mM sodium citrate buffer; pH 4.5) was injected intraperitoneally at 160 mg/kg. Control mice used for determining the normal range of gastric emptying (GE) $t_{1/2}$ values (144 tests in 72 mice) received citrate buffer at an equal volume or remained untreated. After injection, food, oral Similac 10% glucose water (Abbott Laboratories, Chicago, IL) was provided along with unmedicated water for 3 days. In addition, 6 h after injection of streptozotocin, all mice were injected with 300 µL sterile 10% glucose water subcutaneously to prevent a drop in blood glucose due to the release of insulin from disintegrating beta cells. After 3 days, blood glucose and body weight were measured. Mice with blood glucose levels exceeding 500 mg/dL were injected with 1 unit (10 µL) of insulin (Humulin 50/50; Eli Lilly & Co, Indianapolis, IN). Insulin injections were continued depending on blood glucose levels. Mice whose blood glucose levels did not reach 300-400 mg/dL within 7 days of streptozotocin injection were re-injected with streptozotocin using the same protocol up to 3 times.

Collection of blood samples. Approximately 0.015 mL/10 g body weight samples not exceeding 0.1 mL/10g body weight/2 weeks were collected from the submandibular venous plexus under brief manual restraint without anesthesia for the measurement of blood glucose.[9]

Insulin treatment. Diabetic mice with non-fasting blood glucose levels exceeding 500 mg/dL received intraperitoneal insulin treatment to prevent severe hyperglycemia and death.[9] Starting

with a dose of 1 U of an extra-long-acting insulin (Lantus insulin glargine; Aventis Pharmaceuticals Inc., Kansas City, MO), insulin doses were titrated based on daily glucose monitoring. The impact of the insulin was assessed from the blood glucose levels on the following day.

Gastric emptying of solids. Gastric emptying was measured weekly by ^{13}C-octanoic acid breath test,[9-11] a noninvasive, nonrestraining technique. After an overnight fast in a metabolic cage with free access to water, the mice ate 100 mg scrambled cooked egg yolk containing 2.5 µmol ^{13}C-octanoic acid. The mice were then placed in individual gas-tight chambers supplied with cryogenic zero air at approximately 1.5 L/min. Air exiting the chamber containing the exhaled breath was collected and analyzed to determine the ^{13}C/^{12}C ratio using a DLT-100 Carbon Dioxide Isotope Analyzer (Los Gatos Research, San Jose, CA). The sampling rate was 1 Hz and a controlled valve system switched between air flow from up to 12 mouse chambers so that samples were collected from each mouse every 5 min for 6 h. Data were analyzed for GE $t_{1/2}$ and $t_{1/10}$ (the time corresponding to 10% emptying) values using a custom Linux based system.[12] Only the empirical models GVS and GVS2 were used for this study.

In female and male *Nos1$^{creERT2/+}$;Hif1a$^{fl/fl}$* mice, 2 weekly GE $t_{1/2}$ values were averaged before and after tamoxifen or vehicle treatment. In female streptozotocin-diabetic mice, weekly measurements were taken following the experimental design shown in **Figure 2C**. This involved 2 weeks of habituation to the chambers and the instrument, diabetes induction with streptozotocin as described above, and weekly GE tests for up to 12 weeks. Animals with two consecutive delayed GE readings, ie., GE $t_{1/2}$ values exceeding the upper limit (97.5th percentile) of the strain-, age-, and sex-specific normal value, were considered to have gastroparesis.[13] Normal values were as follows: C57BL/6J females (based on 144 tests in 72 mice): 2.5th percentile: 85.33 min, 97.5th percentile: 157.86 min; C57BL/6J males (from 120 tests in 60 mice): 2.5th percentile: 65.20 min; 97.5th percentile: 138.88 min. Diabetic gastroparetic female mice were randomly assigned to vehicle or drug (FG-4592; see below) treatment groups designated as diabetic, delayed, vehicle-treated (DDV) and diabetic, delayed, drug-treated (DDD) groups. Mice that did not develop gastroparesis as defined above by the 8th week post-diabetes were considered “resistant” to gastroparesis and were randomly assigned to vehicle or drug treatment groups designated as diabetic, resistant, vehicle-treated (DRV) and diabetic, resistant, drug-treated (DRD) groups. Treatments continued for 4 weeks with weekly monitoring of GE. The GE $t_{1/2}$ values obtained during the last 3 weeks of the treatment were averaged for each mouse. Treatments were continued until the measurement of gastric volumes (≤26 days).

Measurement of gastric volumes. Gastric volumes were measured noninvasively by single-photon emission computed tomography (SPECT), a method reverse-translated from clinical studies,[14] using U-SPECT-II® scanner with a rotating 75 1mm pinhole collimator (MILabs, Utrecht, Netherlands).[15] After an overnight fast in a metabolic cage with free access to water, the mice were injected intraperitoneally with 100 µCi ^{99m}Tc-pertechnetate in 50 µl. After 20 minutes the mice were anesthetized with isoflurane and placed in the U-SPECT-II scanner. The mice were then allowed to wake up and offered 100 µL of liquid Ensure® that they consumed freely. After consumption, the animals were anesthetized and imaged again between 10 and 15 minutes after meal consumption. Analysis of the SPECT and CT data was done using the PMOD Biomedical Image Quantification and Kinetic Modeling Software (PMOD Technologies, Zurich, Switzerland). The smooth images for both scans were loaded into the program and the maximum counts of both images were adjusted to the lowest value of the smooth data. The volumes of the stomach, defined by thresholding isotope activity to approximately 25% above background activity, were measured in the first and second scan. The change in volume was considered as gastric accommodation.

FG-4592 treatment. Streptozotocin-diabetic mice with or without delayed gastric emptying were treated with FG-4592[16-18] (Roxadustat; 10 mg/kg FG-4592 intraperitoneally once daily for 4 weeks)[19] or vehicle (DMSO:PBS 1:49) starting after 2 consecutive delayed solid gastric emptying results but not later than 8 weeks after the development of diabetes (**Figure 2*C***).

Mouse Euthanasia and Tissue Preparation

Mice were euthanized by CO_2 inhalation anesthesia or by decapitation performed under deep isoflurane (Baxter Healthcare, Deerfield, IL) inhalation anesthesia. Gastric corpus+antrum, small intestinal and colonic tunica muscularis tissues were prepared as described.[20]

Cell Culture

Of cell lines previously reported to express NOS1, we selected the adrenergic mouse neuroblastoma line N1E-115[21] (American Type Culture Collection, Manassas, VA; cat. CRL-2263) for detailed studies because these cells tolerated culturing in the presence of 4% O_2 well. Cells were maintained in Dulbecco's modified Eagle's medium (DMEM) (Thermo Fisher Scientific) containing 450 mg/dL glucose and supplemented with 10% fetal bovine serum (Thermo Fisher Scientific) and 1% penicillin/streptomycin (Thermo Fisher Scientific) at 37°C in a humidified 5% CO_2 atmosphere. Fetal enteric neuron precursor cells (IM-FEN) were the generous gift of Dr. Shanthi K. Srinivasan (Emory University, Atlanta, GA).[22] IM-FEN cells were maintained in modified N-2 medium containing 1% penicillin/streptomycin, GDNF (100 ng/mL; R&D Systems, Minneapolis, MN), 10% fetal bovine serum, and 20 U/mL of recombinant mouse interferon-γ (Sigma-Aldrich) in a humidified tissue culture incubator in the presence of 5% CO_2 at a temperature permissive for the conditionally immortalizing tsA58-mutant SV40 large T antigen (33°C).[22] To further differentiate the IM-FEN cells into neuronal cells, the medium was changed to neurobasal-A medium containing B-27 serum-free supplement (Thermo Fisher Scientific), 1 mmol/L glutamine, 1% penicillin/streptomycin, 1% fetal bovine serum, and GDNF (100 ng/mL) when the confluency reached about 50%-60%, and the cells were cultured at the nonpermissive temperature of 39.5°C.[22] To study the effects of hypoxia, N1E-115 and IM-FEN cells were maintained in the presence of 4% O_2 in a dedicated incubator (NuAire, Plymouth, MN; cat. NU-4950 or Thermo Forma Series II, cat. 3130) for 3 days.

Neuron Sorting

Genetically labeled enteric neurons were isolated and purified from the colon of *Mapt*-EGFP mice and the entire small intestine of tamoxifen-treated *Nos1*$^{creERT2/+}$*;R26*^{mTmG} mice by fluorescence-activated cell sorting (FACS). The muscularis externa of the colon from each *Mapt*-EGFP mouse was pooled together between all mice of the same surgery date (2, 4, and 6 mice) and mechanically and enzymatically dissociated into single cells with a two-step process that first enriches for cells within myenteric ganglia.[23] The pooled cells from each group of mice formed one biological replicate and subjected to FACS immediately after dissociation. Using a Becton Dickinson (Franklin Lakes, NJ) FACSAria IIu instrument running FACSDiva software (see **Supplementary Table 2** for configuration), *Mapt*-EGFP^{+} neurons with or without the CTB-AF647 tracer and *Mapt*-EGFP^{-} non-neuronal cells were sorted from the myenteric cell population after gating out debris and cell clusters based on light scatter and hematopoietic cells labeled with an antibody cocktail targeting the general hematopoietic marker CD45 (PTPRC)

and the macrophage markers CD11b (ITGAM) and F4/80 (ADGRE1) (**Supplementary Figure 1*A*, Supplementary Table 3**). We used a 70 µm nozzle. Threshold was set to 1,000 and doublet discrimination was turned on. Cells isolated from C57BL/6J mice injected with CTB-AF647 or vehicle and vehicle-injected *Mapt*-EGFP mice were used as gating controls. Approximately 135,000 *Mapt*-EGFP^{+}CTB-AF647^{-} neurons/colon were sorted in each of the 3 FACS experiments and frozen for RNA extraction and transcriptome analysis as described below. The frequency of *Mapt*-EGFP^{+}CTB-AF647^{+} neurons was approximately 125-fold lower than that of *Mapt*-EGFP^{+}CTB-AF647^{-} neurons and RNA from these preparations did not pass quality control. Therefore, only data from *Mapt*-EGFP^{+}CTB-AF647^{-} neurons were analyzed and referred to as *Mapt*-EGFP^{+} cells.

Tissues from 6-day tamoxifen-treated *Nos1*$^{creERT2/+}$;*R26*^{mTmG} mice were dissociated using collagenase (Type II; Worthington Biochemical Corporation, Lakewood, NJ; cat. 4176) and previously validated and published methods.[20,24] Single-cell suspensions were fixed to preserve chromatin integrity using the approach described under **Chromatin immunoprecipitation-sequencing (ChIP-seq)** below. Nitrergic neurons in which Cre-mediated recombination led to the expression of membrane-targeted EGFP (*Nos1*-mG^{+} neurons) were sorted on a Becton Dickinson FACSAria II or a FACSAria IIu instrument running FACSDiva v.8.0.1 software (see **Supplementary Table 2** for configurations) using the gating scheme illustrated in **Supplementary Figure 8*F*** (nozzle: 70 µm, threshold: 1,000, doublet discrimination: on). Sort efficiency was 92-93%. Cells isolated from C57BL/6J and untreated, non-recombined *Nos1*$^{creERT2/+}$;*R26*^{mTmG} mice were used as negative controls and *R26*$^{LSL(EGFP)-DTA}$ mice served as positive controls. A total of 3,500,000 small intestinal *Nos1*-mG^{+} neurons were sorted from 16 mice in 3 sessions and pooled for ChIP-seq. Average purity based on reanalysis of aliquots of sorted cells was 87% without adjusting for a slight reduction in fluorescence during the sorting.

Immunohistochemistry, Confocal Microscopy, and Image Analysis

Human tissues. Full thickness tunica muscularis tissues from the gastric corpus of 4 female nondiabetic and 4 female diabetic patients were fixed overnight with 4% paraformaldehyde (PFA), washed 5 times over 1 h in 1x phosphate-buffered saline (PBS) and immersed overnight in 1x PBS solution containing 30% sucrose (Sigma-Aldrich) at 4°C. The specimens were cut in cross-section and frozen in Tissue-Tek OCT Compound (Electron Microscopy Sciences, Hatfield, PA). Frozen samples were sectioned at 12 µm and labeled with anti-HIF1A (Novus Biologicals, Littleton, CO NB-100-134 or Thermo Fisher 700505) and anti-NOS1 (Santa Cruz Biotechnology, Dallas, TX sc-648) antibodies (4°C overnight) and fluorescent-tagged secondary antibodies (Alexa Fluor (AF) 647 donkey anti-rabbit IgG; Jackson ImmunoResearch Laboratories, West Grove, PA 711-605-152 and Cy3 donkey anti-mouse IgG; Millipore AP192C; see **Supplementary Table 3** for details) following a previously established protocol.[25] Nuclei were stained with DAPI (Thermo Fisher D1306; 1:300, 60 min). Sections were mounted with VECTASHIELD HardSet Antifade Mounting Medium (Vector H-1400). Confocal images (12 bits/pixel, 640 x 640 pixels covering a 423.018 µm x 423.018 µm area at a zoom setting of 1.5x or a 317.583 µm x 317.583 µm area at a zoom setting of 2x, one-way scan with line integration (Kalman; count=2)) were acquired using an Olympus (Center Valley, PA) FV1000 system comprised of a BX61 upright microscope, multi-line argon laser, green and red helium-neon lasers, and a 635 nm diode laser and an XLUMPLFL 20x 0.95 NA water immersion objective. The following laser lines, dichroic mirrors (DMs), and filters were used: Channel 1: DAPI: excitation (Ex) DM: DM405/488/543/635, Ex wavelength: 405 nm, emission (Em) DM: SDM490, Em wavelength: 461 nm, Em filter: BA430-470; Channel 2: cyanine 3 (Cy3): Ex DM: DM405/488/543/635, Ex wavelength: 543 nm, Em DM: SDM640, Em filter: BA560-620; and

Channel 3: Alexa Fluor 647: Ex DM: DM405/488/543/635, Ex wavelength: 635 nm, Em DM: mirror, Em wavelength: 668 nm, Em filter: BA655-755. The confocal aperture was 80 µm and the Z step dimension was 1.18 µm/slice. Image stacks were flattened into 2-D maximum intensity projection images and pseudocolored for display using Fluoview v.4.2b application software.

For quantitative image analysis, gastric corpus tissues from 6 nondiabetic patients (3 females and 3 males) and 7 female diabetic patients were fixed with 4% paraformaldehyde for 12 h, dehydrated with 30% sucrose for 12 h, permeabilized with 0.25% Triton X-100 for 50 min and blocked with 10% donkey serum (Jackson ImmunoResearch; see **Supplementary Table 3**) for 1 h at room temperature. The tissues were labeled with anti-HIF1A (Thermo Fisher 700505; rabbit monoclonal) and anti-NOS1 (Santa Cruz Biotechnology sc-648; mouse monoclonal) at a dilution of 1:300 in 5% donkey serum and incubated for 12 hours at 4°C. Alexa Fluor 647 donkey anti-rabbit IgG (Thermo Fisher A31573) and Alexa Fluor 488 donkey anti-mouse IgG (Thermo Fisher A21202) were used as secondary immunoreagents (1:450, 60 min at room temperature). Nuclei were stained with DAPI (Thermo Fisher D1306; 1:300, 60 min). Sections were mounted with VECTASHIELD HardSet Antifade Mounting Medium (Vector H-1400). Images were acquired with a Nikon (Nikon Corporation, Minato City, Japan) AX R confocal system coupled to a Nikon Ti2-E inverted microscope using a Nikon Plan Apo λ 20x lens. The AX R has 8 laser lines (405, 445, 488, 514, 561, 594, 640, and 730nm) in two launches for excitation, a 2k pps resonant and a 8k pps galvano scan head with five detectors including DUX-VB4 detector for NIR, two tunable and one filter-based GaAsP detectors, and one filter-based high-sensitivity PMT capable of 25mm fields-of-view. DAPI, AF488, and AF647 were excited with the 405-nm, 488-nm, and 640-nm laser lines, respectively (DM: DM405/488/561/640) and detected with the following emission filters: 430-475 nm, 499-551 nm, and 663-738 nm, respectively. Z-stack images of immunostained gastric ganglia were captured with NIS-Elements AR 5.41.00 software at a resolution of 295 x 295 x 0.47 µm per pixel using a pinhole size of 0.9 AU at 640 nm. The acquired images were processed using Nikon's NIS-Elements Segmentation AI (Segment.ai) software, which employs advanced machine learning algorithms for image analysis and segmentation. To delineate neuronal regions of interest within the acquired images and extract pixelated/volumetric data, we employed GA3 recipes specifically designed for automated segmentation tasks (**Supplementary Figure 3**). The segmentation process involved adjusting the algorithm parameters to optimize accuracy and minimize background noise. Segmentation was applied to the flattened confocal stacks to obtain cumulative fluorescence values for HIF1A and NOS1 in the same perikarya. We also trained the Segment.ai software to reconstruct the 3-dimensional volume of the $NOS1^+$ perikarya from the confocal stacks. Cumulative pixel intensities were expressed both as values/segmented area and values/segmented volume. Manual validation and refinement of the segmented regions were conducted to ensure accuracy and reliability during the AI training process.

Mouse whole-mount tissues. Whole-mounts of colonic and jejunal tunica muscularis tissues were prepared from *Nos1*^{cre}*;R26*^{nTnG} and tamoxifen- or vehicle-treated *Nos1*$^{creERT2/+}$*;R26*^{nTnG} and *Nos1*$^{creERT2/+}$*;R26*^{mTmG} mice as previously described.[26] PFA fixation and labeling with primary and secondary antibodies to were performed according to established protocols[27] (**Supplementary Table 3**). Membrane-bound or nuclear EGFP and Tomato fluorescence, as well as NOS1, HuC/D, and UCHL1 immunofluorescence in the whole-mounts was visualized by confocal microscopy using an Olympus FV1000 system as described for the human tissues above and

the following settings: 12 bits/pixel, 640 x 640 pixels covering a 635.166 µm x 635.166 µm area at a zoom setting of 1x, one-way scan with line integration (Kalman; count=2), 80 µm confocal aperture, and 1.18 µm/slice Z step dimension. The following laser lines, dichroic mirrors (DMs), and filters were used: Channel 1: EGFP: Ex DM: DM405/488/543/635, Ex wavelength: 488 nm, Em DM: SDM560, Em filter: BA505-525, Channel 2: Tomato: Ex DM: DM405/488/543/635, Ex wavelength: 543 nm, Em DM: SDM640, Em filter: BA560-620; Channel 3: Alexa Fluor 647: Ex DM: DM405/488/543/635, Ex wavelength: 635 nm, Em DM: mirror, Em wavelength: 668 nm, Em filter: BA655-755; and Channel 4: DyLight 405: Ex DM: DM405/488, Ex wavelength: 405 nm, emission (Em) DM: mirror, Em wavelength: 422 nm, Em filter: BA430-470. Image stacks were flattened into 2-D maximum intensity projection images and pseudocolored for display using Fluoview v.4.2b application software.

Analysis of in vivo retention of Hypoxyprobe in mouse cryosections. Intracellular hypoxia was assessed by in vivo Hypoxyprobe (pimonidazole HCl dye; Hypoxyprobe, Inc.) retention in the stomach of STZ-diabetic and nondiabetic C57BL/6J mice. 60 mg/kg pimonidazole HCl (Hypoxyprobe, Inc. Burlington, MA) was administered by intraperitoneal injection 60 minutes prior to euthanasia. Pimonidazole HCl dye retention was detected according to the manufacturer's protocol. Briefly, 5 µm cryosections were prepared from 4% PFA-fixed full-thickness gastric tissues, and pimonidazole adducts were revealed by immunolabeling with DyLight 549-tagged mouse monoclonal antibodies (Hypoxyprobe, Inc.) at 4°C overnight. Nuclei were counterstained with DAPI. The tissues were also labeled with antibodies targeting the neuronal markers NOS1, UCHL1, TUBB3, and the interstitial cell of Cajal marker KIT (**Supplementary Table 3**). 8-bit wide-field fluorescence images (1326 x 998 pixels) of cryosections were captured with a Nikon (Melville, NY) Eclipse TS-100F microscope equipped with a Modulation Optics (Glen Cove, NY) HMC ELWD Plan Fluor 40x, 0.60 NA and HMC ELWD Plan Fluor 20x, 0.45 NA air objectives and a Jenoptik (Brighton, MI) ProgRes MFCool CCD camera and ProgRes Mac CapturePro v. 2.7.6 Software. Samples from mice not injected with pimonidazole served as negative controls.

Analysis of Hypoxyprobe retention in cells. N1E-115 were plated at the concentration of $5x10^4$ cells per 22 mm x 22 mm cover glass (Thermo Fisher Scientific) in 6-well cell culture plates and cultured for one day. After refreshing the culture medium, the coverslips were transferred to the hypoxic incubator (4% O_2) and the cells were cultured for an additional 3 days. 2 hours before fixing the cells, the medium was replaced with fresh medium containing 10 µM Hypoxyprobe (Hypoxyprobe, Inc.). Cultured cells were fixed with 4% PFA, permeabilized with Triton X-100 (Sigma-Aldrich) and immunolabeled for HIF1A using a previously published protocol.[28] 8-bit wide-field fluorescence images (1326 x 998 pixels) were captured using a Nikon (Melville, NY) Eclipse TS-100F fluorescent microscope equipped with Hoffman Modulation Contrast (Glen Cove, NY) objectives and a Jenoptik ProgRes MFCool CCD digital camera and ProgRes Mac CapturePro v. 2.7.6 Software.

Controls and image processing. Specificity of immunolabeling was verified by omitting the primary antibodies, by examining the samples with filter sets not designed for the fluorochrome used, and by analyzing experimental controls lacking the genetically encoded fluorescent proteins. Post-acquisition manipulation of fluorescent images was restricted to assignment of pseudocolor and adjustments to brightness and contrast, which were applied uniformly to the entire images but performed separately in each optical channel if it was necessary for a balanced overlay using Olympus Fluoview v.4.2b or Corel PhotoPaint X5 software (Corel Corporation, Ottawa, ON, Canada). No nonlinear adjustment such as gamma correction was applied to any of the images. Some of the wide-field fluorescent images captured with the Jenoptik camera system were cropped to a square format (998 x 998 pixels) for better

integration into figures and to eliminate blank areas not covered by the tissues. Full-size images are shown in the **Supplementary Material**.

Western Blotting

Tissue and cell lysates were prepared and subjected to sodium dodecyl sulfate (SDS)-polyacrylamide gel electrophoresis and immunoblotting as described previously[26] (see antibodies in **Supplementary Table 3**). Target and reference proteins were detected simultaneously using LI-COR Biosciences (Lincoln, NE) secondary antibodies tagged with near-infrared and infrared fluorescent dyes (IRDye700: red pseudocolor; IRDye800CW: green pseudocolor). Bound antibodies were visualized using an Odyssey XF Infrared Imaging System (LI-COR Bioscience) and Bio-Rad Quantity One 4.5.1 software (Bio-Rad Laboratories, Hercules, CA). Protein bands of interest were expressed in densitometric units normalized to the loading control (glyceraldehyde-3-phosphate dehydrogenase; GAPDH or β-actin; ACTB) detected simultaneously in the same sample and in the same blots. Quantitative comparisons of loading control-normalized data were made between samples acquired and processed independently.

Co-Immunoprecipitation

Protein lysates were incubated with 5-10 µg antibodies (**Supplementary Table 3**) overnight. Non-immune IgG antibody was used as a negative control. The complexes containing the target protein were immunoprecipitated with Protein A/G Agarose (Thermo Fisher Scientific) overnight. Protein in 2x Laemmli Sample Buffer (Bio-Rad) was subjected to gel electrophoresis using 8-10% SDS-PAGE (90 V for 110 min) and transferred to 0.45 µm Immobilon-FL PVDF blotting membranes (Millipore, Billerica, MA). After blocking for 1h at room temperature in LI-COR Odyssey Blocking Buffer (LI-COR Bioscience), the blot was placed in primary antibody solution overnight at 4 °C and secondary, horseradish peroxidase-conjugated antibody solution for 1 h at room temperature (see antibodies in **Supplementary Table 3**). Bands were visualized using SuperSignal™ West Pico Chemiluminescent Substrate (Thermo Fisher Scientific) and imaged using CL-XPosure Film (Thermo Fisher Scientific) (exposure time: 1-3 min).

Quantitative Reverse Transcription-Polymerase Chain Reaction (RT-qPCR)

RT-qPCR was performed using previously published methods[29] and specific, intron-spanning primers (**Supplementary Table 4**). The cDNA was amplified on a Bio-Rad CFX96 or a Roche LightCycler 480 II (Roche Applied Science, Penzberg, Germany) real-time PCR detector using the SYBR GreenER qPCR SuperMix (Thermo Fisher Scientific).

Transcriptome Analysis by Gene Expression Microarrays

Total RNA was isolated from *Mapt*-EGFP^{+} colonic neurons sorted in 3 independent batches from 2, 4, and 6 individual mice using RNA-Bee (AMSBIO, Cambridge, MA) and purified with RNeasy Mini Kit (Qiagen, Germantown, MD). RNA quality was tested using Agilent Electropherogram (Agilent Technologies, Santa Clara, CA). and hybridized to Affymetrix Mouse Genome 430.2 gene expression microarrays (Thermo Fisher Scientific) as described previously.[30] After initial checks for chip quality, probe-level data were pre-processed by robust

multiple-array analysis (RMA), quantile normalization using perfect match probe only, and median polish for probe level signal summarization using R packages. The microarray data have been deposited in a public database (National Center for Biotechnology Information, U.S. National Library of Medicine Gene Expression Omnibus (GEO), https://www.ncbi.nlm.nih.gov/geo/) as part of SuperSeries GSE139483, SubSeries GSE199990. Expression values are in **Supplementary Data 1**.

Transcriptome Analysis by Stranded Total RNA-Sequencing

Total RNA was isolated from N1E-115 cells cultured at 20% O_2 and 4% O_2 (3 independent cultures per condition) and purified using the Qiagen RNeasy Mini Kit. Sequencing libraries were constructed using 100 ng of total RNA and the TruSeq Stranded Total RNA LT (with Ribo-Zero Human/Mouse/Rat) Set A kit (Illumina, San Diego, CA). Libraries were sequenced at 243-303 million fragment reads per sample following Illumina's standard protocol using the Illumina cBot and HiSeq 3000/4000 PE Cluster Kit. The flow cells were sequenced as 101x2 paired-end reads on an Illumina HiSeq 4000 using HiSeq 3000/4000 SBS Kit and HCS v 3.3.52 collection software. Base-calling was performed using Illumina's RTA version 2.7.3. The transcriptome data have been deposited in a public database (National Center for Biotechnology Information, U.S. National Library of Medicine Gene Expression Omnibus (GEO), https://www.ncbi.nlm.nih.gov/gds/) as part of SuperSeries GSE139483, SubSeries GSE139472. Raw total RNA-seq data were analyzed by the MAP-RSeq 3.0.1 pipeline developed by the Mayo Clinic Bioinformatics Core[31] as described previously.[28] Briefly, the pipeline generates detailed quality control data to estimate the distance between paired-end reads, evaluate the sequencing depth for alternate splicing analysis, determine the rate of duplicate reads and to evaluate coverage of reads across genes using the RSeQC software.[32] Paired-end reads were aligned to the mouse genome (mm10) using the Spliced Transcripts Alignment to a Reference (STAR) software package.[33] Gene and exon counts were generated using HTseq software (http://www-huber.embl.de/users/anders/HTSeq/doc/overview.html). RefSeq and Ensembl gene annotations were from http://cole-trapnell-lab.github.io/cufflinks/igenome_table/ (**Supplementary Data 4**). Differential gene expression between N1E-115 cells cultured at 20% O_2 and 4% O_2 was analyzed using the Bioconductor package edgeR.[34] *Nos1* transcripts were assembled using StringTie2.[35]

Gene Set Enrichment and Pathway Analysis

Genes differentially expressed between N1E-115 cells cultured at 20% O_2 and 4% O_2 (P<0.05 and fold change>|1.5|) were subjected to Ingenuity Pathway Analysis (Qiagen) (**Supplementary Data 6**). Differential enrichment of gene sets assembled into matrices was determined by gene set enrichment analysis (GSEA; https://www.gsea-msigdb.org/gsea/index.jsp)[36] applied to the normalized gene expression values (FPKM) (**Supplementary Data 5**). Average FPKM data from cells cultured at 20% O_2 or 4% O_2 were subjected to GSEA Preranked analysis. Mouse genes were remapped to human orthologs before analysis. The gene set matrices interrogated included the Hallmark gene sets in Molecular Signatures Database (MSigDB) 7.4[36] and the custom *Nos1*&Neuron matrix assembled by searching the MSigDB 7.4 for neuronal or neurodegenerative disease-related gene sets containing *Nos1* (**Supplementary Data 2**). Both the standard (differential) and Preranked GSEA analyses were performed using default parameters (see in the worksheets marked as "_RPT" in **Supplementary Data 5**. GSEA Preranked analysis was also applied to average microarray gene expression values obtained from *Mapt*-EGFP$^+$ neurons sorted from 3 individual mouse colons and remapped to human

orthologs (**Supplementary Data 3**). In addition, GSEA Preranked analysis was performed in publicly available bulk total RNA-sequencing results (average $\log_2$ RPKM values of genes remapped to human orthologs) from cyan fluorescent protein-positive duodenal, ileal, and colonic neurons from Tg(Phox2b-HIST2H2BE/Cerulean)1Sout (*Phox2b*-CFP) mice[37] (GSE153202: GSM4634756, GSM4634757, GSM4634760, GSM4634761, GSM4634764, and GSM4634765), and single-cell RNA-sequencing data ($-\log_{10}$ adjusted P values for genes remapped to human orthologs) from Tomato-positive small intestinal neurons from *Baf53b-cre;R26R-Tomato* (*Baf53b*-Tom) mice[38] (clusters EN1-EN12 including the *Nos1*-expressing clusters EN8-EN10) (GSE149524: GSM4504450 and GSM4504451) (**Supplementary Data 3**, see analysis parameters in the worksheets marked as "_RPT").

Chromatin Immunoprecipitation (ChIP) and Chromatin Immunoprecipitation-Sequencing (ChIP-seq)

N1E-115 mouse neuroblastoma cells cultured at 20% O_2 or 4% O_2 for 3 days were treated with 1% formaldehyde (Thermo Fisher Scientific) for 10 min at room temperature to cross-link DNA–protein complexes. The reaction was quenched with 125 mM glycine (5 min, room temperature). Cells were then lysed by incubating in lysis buffer (10 mM Tris-HCl, pH 7.5, 10 mM NaCl, 0.5% NP-40) for 10 minutes at 4°C. The same protocol was applied to the single-cell suspensions obtained from tamoxifen-treated *Nos1*$^{creERT2/+}$;*R26*^{mTmG} mice before the isolation of *Nos1*-mG$^+$ neurons by FACS. Chromatin was first fragmented with micrococcal nuclease at 2000 gel units/mL (New England Biolabs, Ipswich, MA) in digestion buffer (20 mM Tris-HCl, pH 7.5, 15 mM NaCl, 60 mM KCl, 1 mM $CaCl_2$) at 37°C. After 20 min, the reaction was stopped with 2x ChIP buffer (100 mM Tris-HCl, pH 8.1, 20 mM EDTA, 200 mM NaCl, 2% Triton X-100, 0.2% sodium deoxycholate buffer). The chromatin was further fragmented using a Bioruptor sonicator (Diagenode, Denville, NJ; 15 cycles of 30 seconds on and 30 seconds off). Fragment sizes were determined using an Advanced Analytical Technologies (Ankeny, IA) Fragment Analyzer™ Automated CE System. Chromatin preparations were incubated with extensively validated[39] antibodies including in-house-generated, previously published antibodies targeting acetylated histone H3 lysine 9 (H3K9ac)[40,41] and trimethylated H3K4 (H3K4me3)[41,42] (**Supplementary Table 3**) overnight at 4°C and precipitated using Protein-G agarose beads (Roche Diagnostics, Indianapolis, IN). After elution of DNA-protein complexes, crosslinks were reversed by overnight heat treatment (65°C), and proteins were degraded with proteinase K (Ambion, Thermo Fisher Scientific) for 2 hours at 37°C. DNA was purified using Qiagen PCR Purification Kit. Enrichment of target DNA relative to 1% of input DNA was analyzed by SYBR Green real-time PCR (Thermo Fisher Scientific) (**Supplementary Table 5**) or next-generation sequencing. Sequencing libraries were constructed using the NuGEN Ovation Ultralow DR Multiplex System 1-8 (NuGEN Technologies, San Carlos, CA). Briefly, the DNA fragments underwent end repair, barcoded sequencing adapter ligation, purification (Agencourt RNAClean XP beads; Beckman Coulter) and PCR-amplification (13 cycles). Final ChIP libraries were sequenced (paired-end; 51 bases/read) on the Illumina HiSeq 2500 or 4000 platforms. Data were analyzed by the HiChIP pipeline.[43] Briefly, reads were aligned to the mm10 genome assembly using BWA and visualized using Integrative Genomics Viewer (IGV[44]).[45] Mapped reads were post-processed to remove duplicates and pairs of reads mapping to multiple locations. *MACS2*[46,47] and *SICER*[48] algorithms were used for peak-calling in relation to the input DNA. Genomic features of ChIP-seq peaks were analyzed by the Bioconductor package ChIPseeker[49] (https://bioconductor.org/packages/release/bioc/html/ChIPseeker.html). Differentially bound peaks were called using the Bioconductor open-source software DiffBind[50] (https://bioconductor.org/packages/release/bioc/html/DiffBind.html). Super-enhancers were detected with Rank Ordering of Super-Enhancers (*ROSE*) algorithm.[51,52] Epigenetic states were

modelled and predicted using ChromHMM.[53,54] A 20-state and a simplified, 10-state model were built for detailed analysis and easy visualization of *cis*-regulatory elements and other epigenomic features. Chromatin state changes between cells cultured at 20% O_2 and 4% O_2 were summarized and visualized using a Sankey plot.[55] Reproducibility was verified by correlation analysis of biological replicates. Data were visualized in R using plotHeatmap (https://www.rdocumentation.org/packages/seqplots/versions/1.10.2/topics/plotHeatmap). The ChIP-seq data have been deposited in a public database (National Center for Biotechnology Information, U.S. National Library of Medicine Gene Expression Omnibus (GEO), https://www.ncbi.nlm.nih.gov/gds/) as part of SuperSeries GSE139483, SubSeries GSE139477, GSE139478, GSE139479, and GSE139481.

RNA Interference (RNAi)

RNAi against HIFA1 and RAD21 was performed using Dhamacon ON-TARGETplus® SMARTpool® small interfering RNAs (siRNAs) or corresponding scrambled sequences (25 nM) and DharmaFECT1 Transfection Reagent (Thermo Fisher Scientific) according to manufacturer's protocol. Treatment was applied following one-day culturing in antibiotic- and antimycotic-free media. Knock-down efficacy was assessed after 72 hours by Western blotting.

Luciferase Assay

Genomic DNA was prepared from mouse N1E-115 cells. *Nos1* promoter fragments (mm10 chr5:117,780,715-117,782,330, chr5:117,790,371-117,791,488 and chr5:117,841,682-117,843,201) were PCR-amplified and subcloned into pGL3-Enhancer luciferase reporter vectors (Promega U47297; Promega Corporation, Madison, WI), whereas their cognate enhancers (mm10 chr5:117,779,022-117,780,534, chr5:117,789,325-117,790,863, chr5:117,836,566-117,838,048, chr5:117,838,359-117,839,255 and chr5:117,840,197-117,841,068) were PCR-amplified and subcloned into pGL3-Promoter luciferase reporter vectors (Promega U47298). pGL3-Basic (Promega U47295; negative control), pGL3-Control (Promega U47296; positive control) or cloned vectors were transfected into N1E-115 cells together with the Renilla luciferase control co-reporter (pRL-TK) vector (Promega Corporation) as a constitutively active internal control using Lipofectamine LTX or Lipofectamine 3000 (Thermo Fisher Scientific). 24 hours after transfection, the cells were harvested and lysed for 20 minutes, Firefly luciferase activity was measured using the dual luciferase assay (Promega Corporation) implemented on a Promega GloMax Plate Reader (Promega Corporation) and normalized to Renilla luciferase activity.

Clustered, Regularly Interspaced Short Palindromic Repeats (CRISPR)-CRISPR-Associated Protein 9 (CRISPR-Cas9)-Mediated Genomic Deletion

CRISPR RNAs (crRNAs) targeted to loci flanking targeted *cis*-regulatory regions (E1: mm10 chr5:117,778,575-117,780,386; P1: mm10 chr5:117,780,619-117,783,412; P3: mm10 chr5:117,841,950-117,843,952) were designed on benchling.com and obtained from Integrated DNA Technologies (Coralville, IA) (**Supplementary Table 1**). crRNAs were annealed with trans-activating CRISPR RNA (tracrRNA) (Integrated DNA Technologies) and delivered into cells together with Cas9 protein (Integrated DNA Technologies) using Lipofectamine RNAiMAX Transfection Reagent (Thermo Fisher Scientific). Deletions were detected by genomic PCR (**Supplementary Table 1**). Single-cell clones with deletion were generated by sib-selection.[56]

Chromosome Conformation Capture (3C)

N1E-115 mouse neuroblastoma cells were cultured at 20% O_2 and 4% O_2 for 3 days, cross-linked with 1% formaldehyde and quenched by 2.5 mol/L glycine. Cells were resuspended in 10 mL lysis buffer (10 mmol/L Tris-HCl, pH 7.5, 3 mmol/L $CaCl_2$, 2 mmol/L $MgCl_2$, 10 mmol/L NaCl, 0.2% NP40) with Protease inhibitor (Sigma-Aldrich) and 5 mmol/L PMSF (Sigma-Aldrich). The cell suspension was washed with 1.2x NE Buffer 2.1 (New England Biolabs), resuspended in 0.5% SDS, incubated at 37°C for 50 min then at 65°C for 10 min. After quenching the SDS, the chromatin was digested overnight by 600 U *Nco*I (New England Biolabs) at 37°C and then ligated with 400 U T4 ligase (Thermo Fisher Scientific) at 16°C for 4 hours. Ligated DNA was purified using phenol-chloroform (Sigma-Aldrich) and ethanol after incubating with 30 µL 10 mg/mL Protease K (Thermo Fisher Scientific) for 3 hours at 55°C and overnight at 65°C, and with 30 µL 10 mg/ml RNase A (Thermo Fisher Scientific) for 30 min at 37°C. Taqman Quantitative PCR was performed using PrimeTime Gene Expression Master Mix (Integrated DNA Technologies) with custom probe and primers as described previously.[57] We used bacterial artificial chromosome[58] RPCI-23-379F5 as normalization control. BAC-normalized data were then scaled to a range of 0-1 across the loci tested to facilitate comparison between data obtained at 4% O_2 and 20% O_2. Probe and primer sequences are shown in **Supplementary Table 6**.

Genome-Wide Chromosome Conformation Capture (HiC)

We performed two independent chromosome conformation capture-sequencing (HiC) experiments utilizing the Arima, Inc. (San Diego, CA) 2-enzyme chemistry that digests chromatin at ^GATC and G^ANTC, where N can be any of the 4 genomic bases, and *Nco*I digestion following a published HiC protocol.[59] N1E-115 mouse neuroblastoma cells were cultured at 20% O_2 and 4% O_2 for 3 days, cross-linked with 1% formaldehyde and quenched by 2.5 mol/L glycine. In the first study, cells were resuspended in lysis buffer provided in the Arima HiC kit, digested, labeled with biotin, and ligated according to the protocol provided by the manufacturer. Briefly, 75 ng of crosslinked DNA in 50 µL elution buffer and the QC beads provided with the Arima HiC kit were used for Arima QC1 Quality Control. The chromatin samples were sheared to an average size of 300-400 bp using a Bioruptor Pico sonicator (Diagenode), and size selection was performed using AMPure XP paramagnetic beads (Beckman Coulter, Indianapolis, IN). Biotin enrichment, end repair, dA-tailing, and adapter ligation were performed according to the Arima HiC Kit. Libraries were prepared using KAPA Hyper Prep kit (Roche Diagnostics). The KAPA Library Quantification Kit (Roche Diagnostics) was utilized to determine the Arima QC2 values and estimate the appropriate number of PCR cycles needed for library amplification. Libraries were subjected to paired-end sequencing[60] on the Illumina HiSeq 4000 platform.

Replicate experiments were performed using a conventional HiC protocol.[59,61] N1E-115 mouse neuroblastoma cells were cultured at 20% O_2 and 4% O_2 for 3 days, cross-linked with 1% formaldehyde and quenched by 2.5 mol/L glycine. Cells were resuspended in ice-cold lysis buffer (10 mM Tris-HCl pH8.0, 10 mM NaCl, 0.2% Igepal CA-630) containing protease inhibitor cocktail and digested overnight at 37°C with 800 U *Nco*I (New England Biolabs; cat. R3193). DNA was labeled with biotin-14-dCTP by adding 60 µL fill-in mastermix to the sample (0.4 mM biotin-14-dCTP, 10 mM dATP, 10 mM dGTP, 10 mM dTTP (Thermo Fisher Scientific), 5 U/µl Klenow DNA polymerase, and 6 µL 10x NEBuffer 2 (New England Biolabs)) and ligated with

400 U T4 DNA ligase (Thermo Fisher Scientific) at 16°C overnight. With a successful biotin fill-in, *Nco*I restriction sites (CCATGG) are converted into NsiI sites (ATGCAT). To test the efficiency of this process, we used PCR to amplify a ligation product formed by two nearby restriction fragments followed by digestion with *Nco*I (New England BioLabs), *Nsi*I (New England BioLabs) and by a double digestion with *Nco*I+*Nsi*I restriction enzymes. The primers used for PCR were: P2-F: actcccacaaggaccagcta; E3-R: ggagttgcaggactcaggtc. Biotin from unligated ends was removed with 3,000 U/ml T4 DNA polymerase (New England BioLabs). The chromatin samples were sheared to an average size of 300-400 bp using a Bioruptor Pico sonicator (Diagenode) and subjected to size selection using AMPure XP beads (Beckman Coulter). Ends were repaired using 5 U/µl Klenow DNA polymerase, 10 U/µl T4 polynucleotide kinase, 3 U/µl T4 DNA polymerase (all from New England BioLabs), and 2.5 mM dNTP mix (Thermo Fisher Scientific) in 10x ligation buffer (New England BioLabs). DNA was purified using QIAGEN MinElute columns (Qiagen). A-tailing of the purified DNA was performed using Klenow fragment (3'→5' exo-) (New England BioLabs). HiC DNA products were pulled down using Dynabeads MyOne Streptavidin C1 (Thermo Fisher Scientific). Illumina paired-end adapter was ligated to DNA bound to streptavidin beads and paired-end PCR was performed using *Pfu*Ultra II Fusion DNA polymerase (Agilent). HiC libraries were sequenced on the Illumina HiSeq 4000 platform. Data were analyzed by HiC-Pro[62] and visualized using Juicebox.[63] Chromatin loops were identified by HiC Computational Unbiased Peak Search (HiCCUPS), contact domains were detected by Arrowhead, and the aggregate enrichment of a set of putative two-dimensional peaks was measured by aggregate peak analysis (APA).[64] The HiC data have been deposited in a public database (National Center for Biotechnology Information, U.S. National Library of Medicine Gene Expression Omnibus (GEO), https://www.ncbi.nlm.nih.gov/geo/) as part of SuperSeries GSE139483, SubSeries GSE139470.

Statistical Analysis

Hypothesis testing on low-throughput data obtained from distinct samples was performed with the aid of GraphPad Prism 9.3.1 (Dotmatics, Boston, MA) or SigmaPlot 14.5 (SPSS, Chicago, IL) using nonparametric tests (Mann-Whitney U test, Wilcoxon signed rank tests including one-sample and matched-pairs Wilcoxon tests, and Kruskal-Wallis ANOVA on ranks). One-sample *t* test and ratio-paired *t* test were used when normal distribution was verified by the Shapiro-Wilk test. Linearity for linear regression analysis was verified by runs test. Post-hoc multiple comparisons were performed using Dunn's or Tukey's test. Two-tailed tests were used for all tests with symmetrical distribution of the test statistic for the analysis. *P* values are exact values except in the case of Kruskal-Wallis ANOVA on ranks, where approximate *P* values were computed. Unless otherwise stated, data are displayed as scatter plots of all data combined with mean±SD or truncated violin plots with the median and quartiles shown. RNA-seq and ChIP-seq data were analyzed as described in the relevant sections above. For high-throughput data, *P* values adjusted for false discovery rate are reported as *Q* values.

Supplementary References

1. Tucker KL, Meyer M, Barde YA. Neurotrophins are required for nerve growth during development. Nat Neurosci 2001;4:29-37.
2. **Leshan RL**, **Greenwald-Yarnell M**, Patterson CM, et al. Leptin action through hypothalamic nitric oxide synthase-1-expressing neurons controls energy balance. Nat Med 2012;18:820-823.
3. Rupp AC, Allison MB, Jones JC, et al. Specific subpopulations of hypothalamic leptin receptor-expressing neurons mediate the effects of early developmental leptin receptor deletion on energy balance. Mol Metab 2018;14:130-138.
4. **Luo L**, **Ambrozkiewicz MC**, Benseler F, et al. Optimizing Nervous System-Specific Gene Targeting with Cre Driver Lines: Prevalence of Germline Recombination and Influencing Factors. Neuron 2020;106:37-65 e35.
5. Taniguchi H, He M, Wu P, et al. A resource of Cre driver lines for genetic targeting of GABAergic neurons in cerebral cortex. Neuron 2011;71:995-1013.
6. Muzumdar MD, Tasic B, Miyamichi K, et al. A global double-fluorescent Cre reporter mouse. Genesis 2007;45:593-605.
7. Varia MA, Calkins-Adams DP, Rinker LH, et al. Pimonidazole: a novel hypoxia marker for complementary study of tumor hypoxia and cell proliferation in cervical carcinoma. Gynecol Oncol 1998;71:270-277.
8. Gross MW, Karbach U, Groebe K, et al. Calibration of misonidazole labeling by simultaneous measurement of oxygen tension and labeling density in multicellular spheroids. Int J Cancer 1995;61:567-573.
9. Cipriani G, Gibbons SJ, Miller KE, et al. Change in Populations of Macrophages Promotes Development of Delayed Gastric Emptying in Mice. Gastroenterology 2018;154:2122-2136 e2112.
10. Hayashi Y, Toyomasu Y, Saravanaperumal SA, et al. Hyperglycemia Increases Interstitial Cells of Cajal via MAPK1 and MAPK3 Signaling to ETV1 and KIT, Leading to Rapid Gastric Emptying. Gastroenterology 2017;153:521-535 e520.
11. Miller KE, Bajzer Z, Hein SS, et al. High temporal resolution gastric emptying breath tests in mice. Neurogastroenterol Motil 2018:e13333.
12. Bajzer Z, Gibbons SJ, Coleman HD, et al. A gamma variate model that includes stretched exponential is a better fit for gastric emptying data from mice. Am J Physiol Gastrointest Liver Physiol 2015;309:G162-170.
13. Choi KM, Gibbons SJ, Nguyen TV, et al. Heme Oxygenase-1 Protects Interstitial Cells of Cajal From Oxidative Stress and Reverses Diabetic Gastroparesis. Gastroenterology 2008;135:2055-2064.
14. Wang XJ, Burton DD, Breen-Lyles M, et al. Gastric accommodation influences proximal gastric and total gastric emptying in concurrent measurements conducted in healthy volunteers. Am J Physiol Gastrointest Liver Physiol 2021;320:G759-G767.
15. van der Have F, Vastenhouw B, Ramakers RM, et al. U-SPECT-II: An Ultra-High-Resolution Device for Molecular Small-Animal Imaging. J Nucl Med 2009;50:599-605.
16. Chen N, Hao C, Liu BC, et al. Roxadustat Treatment for Anemia in Patients Undergoing Long-Term Dialysis. N Engl J Med 2019;381:1011-1022.
17. Chen N, Hao C, Peng X, et al. Roxadustat for Anemia in Patients with Kidney Disease Not Receiving Dialysis. N Engl J Med 2019;381:1001-1010.
18. Kaplan JM. Roxadustat for Anemia in Patients with Chronic Kidney Disease. Reply. N Engl J Med 2020;383:e3.

19. **Yang Y**, **Yu X**, Zhang Y, et al. Hypoxia-inducible factor prolyl hydroxylase inhibitor roxadustat (FG-4592) protects against cisplatin-induced acute kidney injury. Clin Sci (Lond) 2018;132:825-838.
20. **Lorincz A**, **Redelman D**, Horvath VJ, et al. Progenitors of interstitial cells of Cajal in the postnatal murine stomach. Gastroenterology 2008;134:1083-1093.
21. Amano T, Richelson E, Nirenberg M. Neurotransmitter synthesis by neuroblastoma clones (neuroblast differentiation-cell culture-choline acetyltransferase-acetylcholinesterase-tyrosine hydroxylase-axons-dendrites). Proc Natl Acad Sci U S A 1972;69:258-263.
22. Anitha M, Joseph I, Ding X, et al. Characterization of fetal and postnatal enteric neuronal cell lines with improvement in intestinal neural function. Gastroenterology 2008;134:1424-1435.
23. Melo CGS, Nicolai EN, Alcaino C, et al. Identification of intrinsic primary afferent neurons in mouse jejunum. Neurogastroenterol Motil 2020;32:e13989.
24. **Bardsley MR**, **Horvath VJ**, Asuzu DT, et al. Kitlow stem cells cause resistance to Kit/platelet-derived growth factor alpha inhibitors in murine gastrointestinal stromal tumors. Gastroenterology 2010;139:942-952.
25. Grover M, Farrugia G, Lurken MS, et al. Cellular changes in diabetic and idiopathic gastroparesis. Gastroenterology 2011;140:1575-1585 e1578.
26. Asuzu DT, Hayashi Y, Izbeki F, et al. Generalized neuromuscular hypoplasia, reduced smooth muscle myosin and altered gut motility in the klotho model of premature aging. Neurogastroenterol Motil 2011;23:e309-323.
27. Colmenares Aguilar MG, Mazzone A, Eisenman ST, et al. Expression of the regulated isoform of the electrogenic Na(+)/HCO3(-) cotransporter, NBCe1, is enriched in pacemaker interstitial cells of Cajal. Am J Physiol Gastrointest Liver Physiol 2021;320:G93-G107.
28. Hayashi Y, Asuzu DT, Bardsley MR, et al. Wnt-induced, TRP53-mediated Cell Cycle Arrest of Precursors Underlies Interstitial Cell of Cajal Depletion During Aging. Cell Mol Gastroenterol Hepatol 2021;11:117-145.
29. Horvath VJ, Vittal H, Lorincz A, et al. Reduced stem cell factor links smooth myopathy and loss of interstitial cells of Cajal in murine diabetic gastroparesis. Gastroenterology 2006;130:759-770.
30. Chen H, Ordog T, Chen J, et al. Differential gene expression in functional classes of interstitial cells of Cajal in murine small intestine. Physiol Genomics 2007;31:492-509.
31. **Kalari KR**, **Nair AA**, Bhavsar JD, et al. MAP-RSeq: Mayo Analysis Pipeline for RNA sequencing. BMC Bioinformatics 2014;15:224.
32. Wang L, Wang S, Li W. RSeQC: quality control of RNA-seq experiments. Bioinformatics 2012;28:2184-2185.
33. Dobin A, Davis CA, Schlesinger F, et al. STAR: ultrafast universal RNA-seq aligner. Bioinformatics 2013;29:15-21.
34. **McCarthy DJ**, **Chen Y**, Smyth GK. Differential expression analysis of multifactor RNA-Seq experiments with respect to biological variation. Nucleic Acids Res 2012;40:4288-4297.
35. Kovaka S, Zimin AV, Pertea GM, et al. Transcriptome assembly from long-read RNA-seq alignments with StringTie2. Genome Biol 2019;20:278.
36. **Subramanian A**, **Tamayo P**, Mootha VK, et al. Gene set enrichment analysis: A knowledge-based approach for interpreting genome-wide expression profiles. Proceedings of the National Academy of Sciences of the United States of America 2005;102:15545-15550.

37. May-Zhang AA, Tycksen E, Southard-Smith AN, et al. Combinatorial Transcriptional Profiling of Mouse and Human Enteric Neurons Identifies Shared and Disparate Subtypes In Situ. Gastroenterology 2021;160:755-770 e726.
38. **Morarach K**, **Mikhailova A**, Knoflach V, et al. Diversification of molecularly defined myenteric neuron classes revealed by single-cell RNA sequencing. Nat Neurosci 2021;24:34-46.
39. **Landt SG**, **Marinov GK**, **Kundaje A**, et al. ChIP-seq guidelines and practices of the ENCODE and modENCODE consortia. Genome Res 2012;22:1813-1831.
40. Philips RL, Lee JH, Gaonkar K, et al. HDAC3 restrains CD8-lineage genes to maintain a bi-potential state in CD4(+)CD8(+) thymocytes for CD4-lineage commitment. Elife 2019;8.
41. Puthanmadhom Narayanan S, Lee JH, Bhagwate A, et al. Epigenetic Alterations Are Associated With Gastric Emptying Disturbances in Diabetes Mellitus. Clin Transl Gastroenterol 2020;11:e00136.
42. Zhong J, Ye Z, Lenz SW, et al. Purification of nanogram-range immunoprecipitated DNA in ChIP-seq application. BMC Genomics 2017;18:985.
43. Yan H, Evans J, Kalmbach M, et al. HiChIP: a high-throughput pipeline for integrative analysis of ChIP-Seq data. BMC Bioinformatics 2014;15:280.
44. Robinson JT, Thorvaldsdottir H, Winckler W, et al. Integrative genomics viewer. Nature biotechnology 2011;29:24-26.
45. Robinson JT, Thorvaldsdottir H, Winckler W, et al. Integrative genomics viewer. Nat Biotechnol 2011;29:24-26.
46. Liu T. Use model-based Analysis of ChIP-Seq (MACS) to analyze short reads generated by sequencing protein-DNA interactions in embryonic stem cells. Methods Mol Biol 2014;1150:81-95.
47. **Zhang Y**, **Liu T**, Meyer CA, et al. Model-based analysis of ChIP-Seq (MACS). Genome Biol 2008;9:R137.
48. Zang C, Schones DE, Zeng C, et al. A clustering approach for identification of enriched domains from histone modification ChIP-Seq data. Bioinformatics 2009;25:1952-1958.
49. Yu G, Wang LG, He QY. ChIPseeker: an R/Bioconductor package for ChIP peak annotation, comparison and visualization. Bioinformatics 2015;31:2382-2383.
50. Ross-Innes CS, Stark R, Teschendorff AE, et al. Differential oestrogen receptor binding is associated with clinical outcome in breast cancer. Nature 2012;481:389-393.
51. **Loven J**, **Hoke HA**, **Lin CY**, et al. Selective inhibition of tumor oncogenes by disruption of super-enhancers. Cell 2013;153:320-334.
52. **Whyte WA**, **Orlando DA**, **Hnisz D**, et al. Master transcription factors and mediator establish super-enhancers at key cell identity genes. Cell 2013;153:307-319.
53. Ernst J, Kellis M. ChromHMM: automating chromatin-state discovery and characterization. Nat Methods 2012;9:215-216.
54. Ernst J, Kellis M. Chromatin-state discovery and genome annotation with ChromHMM. Nat Protoc 2017;12:2478-2492.
55. **Bao X**, **Shi R**, Zhao T, et al. Immune landscape and a novel immunotherapy-related gene signature associated with clinical outcome in early-stage lung adenocarcinoma. J Mol Med (Berl) 2020;98:805-818.
56. Miyaoka Y, Chan AH, Judge LM, et al. Isolation of single-base genome-edited human iPS cells without antibiotic selection. Nature Methods 2014;11:291-U345.
57. Hagege H, Klous P, Braem C, et al. Quantitative analysis of chromosome conformation capture assays (3C-qPCR). Nature Protocols 2007;2:1722-1733.
58. Garella R, Squecco R, Baccari MC. Site-related Effects of Relaxin in the Gastrointestinal Tract Through Nitric Oxide Signalling: An Updated Report. Current Protein & Peptide Science 2017;18:1254-1262.

59. **Imakaev M**, **Fudenberg G**, McCord RP, et al. Iterative correction of Hi-C data reveals hallmarks of chromosome organization. Nat Methods 2012;9:999-1003.
60. **van Berkum NL**, **Lieberman-Aiden E**, **Williams L**, et al. Hi-C: a method to study the three-dimensional architecture of genomes. J Vis Exp 2010.
61. Lieberman-Aiden E, van Berkum NL, Williams L, et al. Comprehensive mapping of long-range interactions reveals folding principles of the human genome. Science 2009;326:289-293.
62. **Servant N**, **Varoquaux N**, Lajoie BR, et al. HiC-Pro: an optimized and flexible pipeline for Hi-C data processing. Genome Biol 2015;16:259.
63. Robinson JT, Turner D, Durand NC, et al. Juicebox.js Provides a Cloud-Based Visualization System for Hi-C Data. Cell Syst 2018;6:256-258 e251.
64. **Durand NC**, **Shamim MS,** Machol I, et al. Juicer Provides a One-Click System for Analyzing Loop-Resolution Hi-C Experiments. Cell Syst 2016;3:95-98.

Author names in bold designate shared co-first authorship.

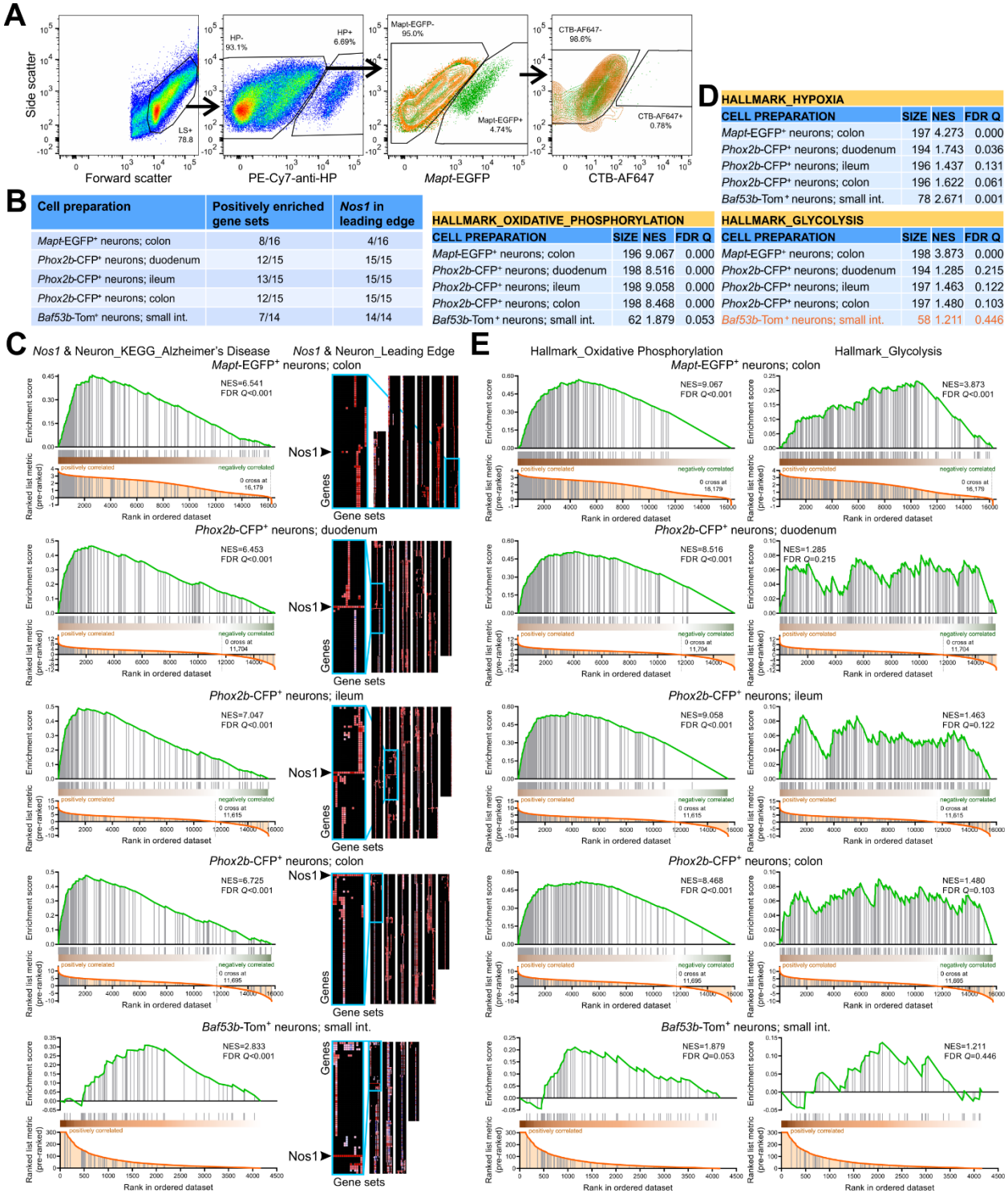

B

Cell preparation	Positively enriched gene sets	*Nos1* in leading edge
Mapt-EGFP⁺ neurons; colon	8/16	4/16
Phox2b-CFP⁺ neurons; duodenum	12/15	15/15
Phox2b-CFP⁺ neurons; ileum	13/15	15/15
Phox2b-CFP⁺ neurons; colon	12/15	15/15
Baf53b-Tom⁺ neurons; small int.	7/14	14/14

D

HALLMARK_HYPOXIA			
CELL PREPARATION	SIZE	NES	FDR Q
Mapt-EGFP⁺ neurons; colon	197	4.273	0.000
Phox2b-CFP⁺ neurons; duodenum	194	1.743	0.036
Phox2b-CFP⁺ neurons; ileum	196	1.437	0.131
Phox2b-CFP⁺ neurons; colon	196	1.622	0.061
Baf53b-Tom⁺ neurons; small int.	78	2.671	0.001

HALLMARK_OXIDATIVE_PHOSPHORYLATION			
CELL PREPARATION	SIZE	NES	FDR Q
Mapt-EGFP⁺ neurons; colon	196	9.067	0.000
Phox2b-CFP⁺ neurons; duodenum	198	8.516	0.000
Phox2b-CFP⁺ neurons; ileum	198	9.058	0.000
Phox2b-CFP⁺ neurons; colon	198	8.468	0.000
Baf53b-Tom⁺ neurons; small int.	62	1.879	0.053

HALLMARK_GLYCOLYSIS			
CELL PREPARATION	SIZE	NES	FDR Q
Mapt-EGFP⁺ neurons; colon	198	3.873	0.000
Phox2b-CFP⁺ neurons; duodenum	194	1.285	0.215
Phox2b-CFP⁺ neurons; ileum	197	1.463	0.122
Phox2b-CFP⁺ neurons; colon	197	1.480	0.103
Baf53b-Tom⁺ neurons; small int.	58	1.211	0.446

Supplementary Figure 1. Hypoxic signaling is active in enteric neurons. (*A*) Gating scheme to enrich *Mapt*-EGFP⁺ colonic neurons by FACS (*n*=2, 4, and 6 mice/biological replicate). CTB-AF647⁺ intestinofugal neurons, which were excluded from the ~135,000 neurons studied, represented ~1.1% of the *Mapt*-EGFP⁺ cells (right panel). (*B*) Enrichment of *Nos1*-related gene sets from the *Nos1*&Neuron gene set matrix detected by pre-ranked GSEA in sorted *Mapt*-EGFP⁺ colonic neurons, *Phox2b*-CFP⁺ small intestinal and colonic neurons[37], and

Baf53b-Tom^{+} colonic neurons[38]. Cutoff: FDR<0.25. (*C*) Left panels: Pre-ranked GSEA plots of Alzheimer's disease-related gene expression from the *Nos1*&Neuron gene set matrix in enteric neurons isolated by FACS. Right panels: heat maps of GSEA leading edge analysis results. See genes and gene sets in **Supplementary Data 3** worksheets labeled "_NOS1&NEURON_LE". The region containing *Nos1* (arrowhead) is enlarged on the left side of the panel. (*D*) Enrichment of hypoxia-, OXPHOS-, and glycolysis-related gene sets from the MSigDB Hallmark v.7.4 gene set matrix detected by pre-ranked GSEA in enteric neurons sorted by FACS. (*E*) Pre-ranked GSEA plots of OXPHOS- and glycolysis-related gene expression from the MSigDB Hallmark v.7.4 gene set matrix in enteric neurons isolated by FACS.

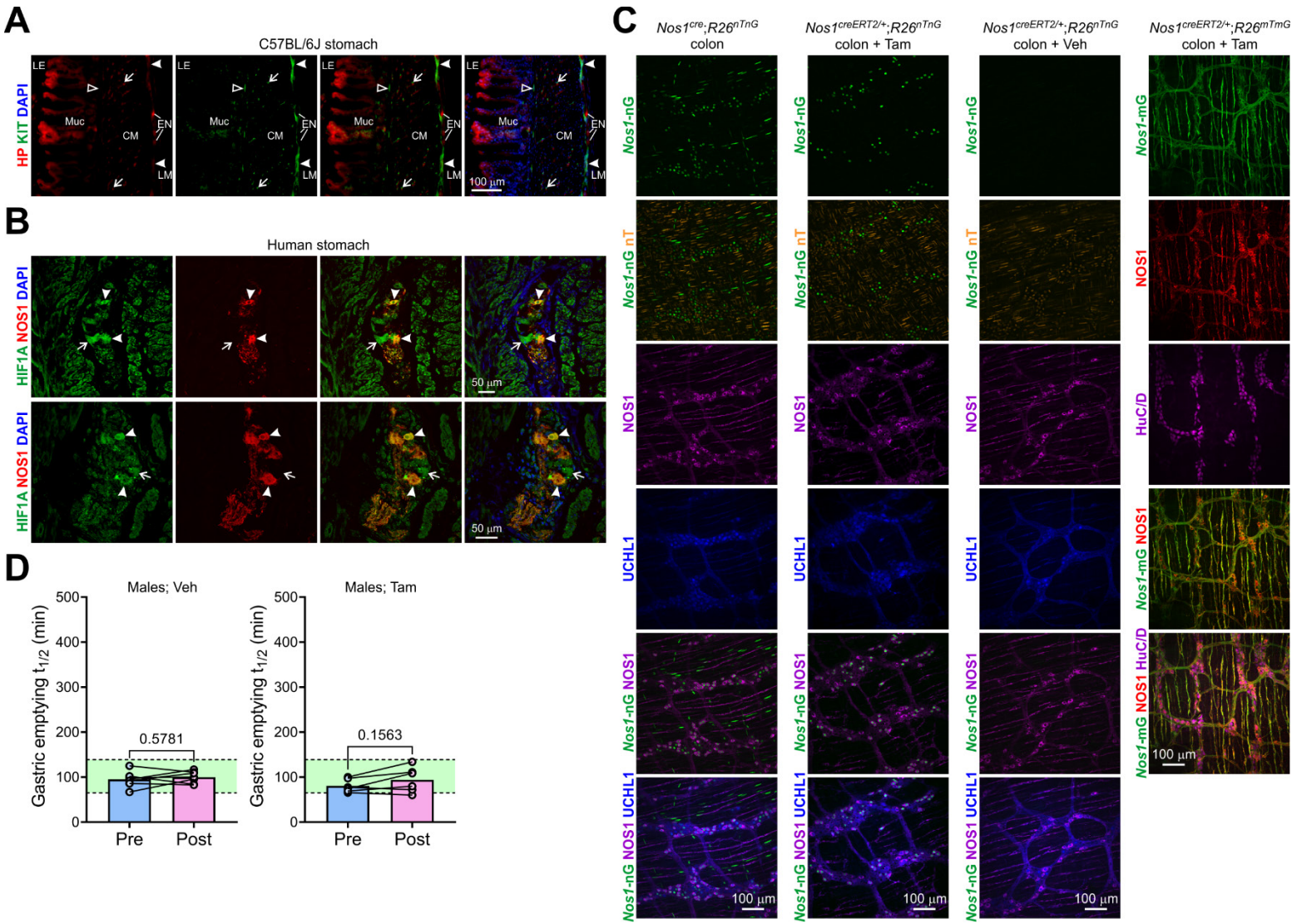

Supplementary Figure 2. Hypoxic signaling in the mouse and human stomach, genetic labeling strategies for nitrergic neurons, and resistance of GE to *Hif1a* deletion in nitrergic neurons in male mice. (*A*) A cryosection of a nondiabetic mouse stomach immunolabeled for in vivo administered Hypoxyprobe (HP) and the ICC marker KIT (representative images from 2 mice). DAPI, 4',6-diamidino-2-phenylindole. Pseudocolored wide-field fluorescent images are shown. LE, luminal epithelium; Muc, mucosa,

CM, circular muscle, LM, longitudinal muscle, EN, enteric neurons. Open arrowheads, submucosal border ICC; arrows, intramuscular ICC, closed arrowheads, myenteric ICC. (*B*) HIF1A immunostaining (primary antibody: Novus Biologicals NB-100-134) in $NOS1^+$ (arrowhead) and $NOS1^-$ (arrow) neurons in cryosections of human stomachs. Representative flattened, pseudocolored confocal Z-stacks from 4 obese, nondiabetic patients are shown. (*C*) Validation of genetic labeling of *Nos1*-expressing cells in colonic tunica muscularis whole-mounts of $Nos1^{cre};R26^{nTnG}$ and tamoxifen (Tam)- or vehicle (Veh)-treated $Nos1^{creERT2/+};R26^{nTnG}$ and $Nos1^{creERT2/+};R26^{mTmG}$ mice. Tissues were counterstained for NOS1 and the general enteric neuronal markers UCHL1 or HuC/D. Representative flattened, pseudocolored confocal Z-stacks from 4 $Nos1^{cre};R26^{nTnG}$, 2 $Nos1^{creERT2/+};R26^{nTnG}$ and 2 $Nos1^{creERT2/+};R26^{mTmG}$ mice are shown. Red+green and red+green+blue images in panels *A* and *B* and the orange+green, magenta+green, red+green, magenta+green+blue, and magenta+red+green images in *C* are digital overlays. Note that in $Nos1^{cre}$ mice, recombination occurred not only in $NOS1^+$ myenteric neurons but also in $NOS1^-$ cells, possibly due to germ line recombination. Because recombination in $Nos1^{creERT2/+}$ mice was limited to $NOS1^+$ neurons, we used this strain for the conditional deletion of *Hif1a*. (*D*) No effect on GE $t_{1/2}$ of genomic deletion of *Hif1a* in vehicle (Veh)- or tamoxifen (Tam)-treated $Nos1^{creERT2/+};Hif1a^{fl/fl}$ mice (n_{Veh}=7; n_{Tam}=6). Green area: strain- and sex-specific normal range (2.5^{th}-97.5^{th} percentile). *P*, ratio-paired *t* tests.

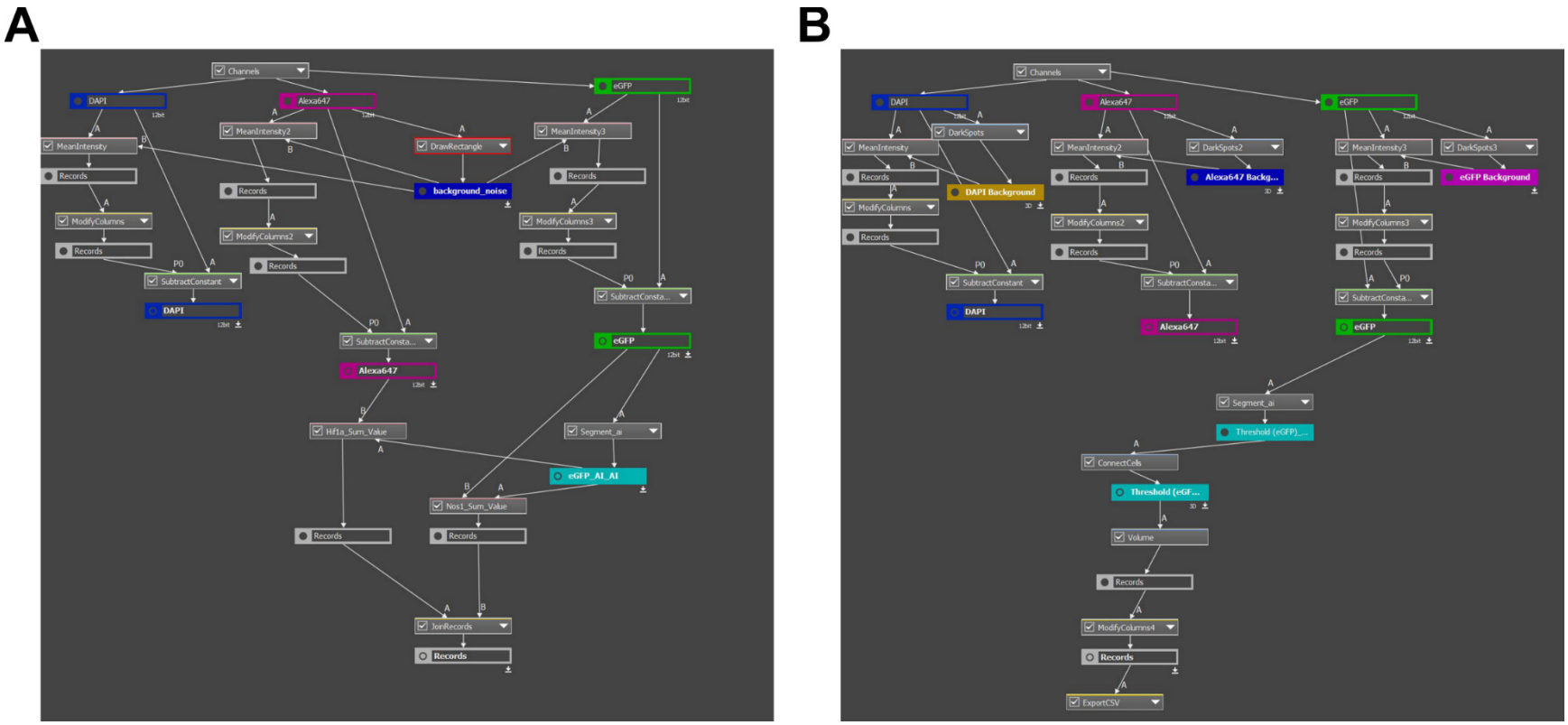

Supplementary Figure 3. Quantitative image analysis workflow diagrams. (*A*) GA3 recipe for obtaining cumulative fluorescence intensities within flattened segmented areas of nitrergic neurons using Nikon's Segment.ai algorithm. (*B*) GA3 recipe for obtaining the volumes of segmented areas across optical sections containing the entire nitrergic perikarya using Nikon's Segment.ai algorithm.

A *Nos1* & Neuron_GSEA Summary

Condition	Positively enriched gene sets	*Nos1* in leading edge
N1E-115; 20% O_2	7/15	9/15
N1E-115; 4% O_2	10/14	11/14
N1E-115; 4% O_2 vs. 20% O_2	10/16 (4% O_2) 0/16 (20% O_2)	16/16 N/A

Nos1 & Neuron Leading_Edge

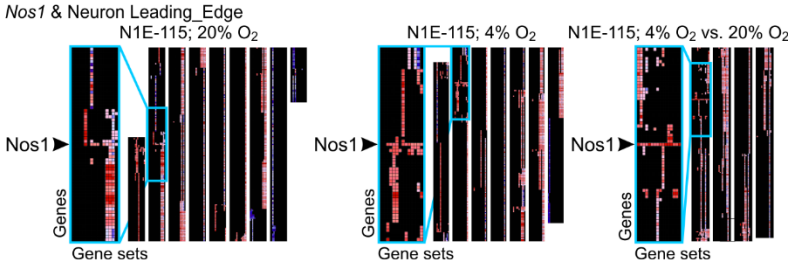

B

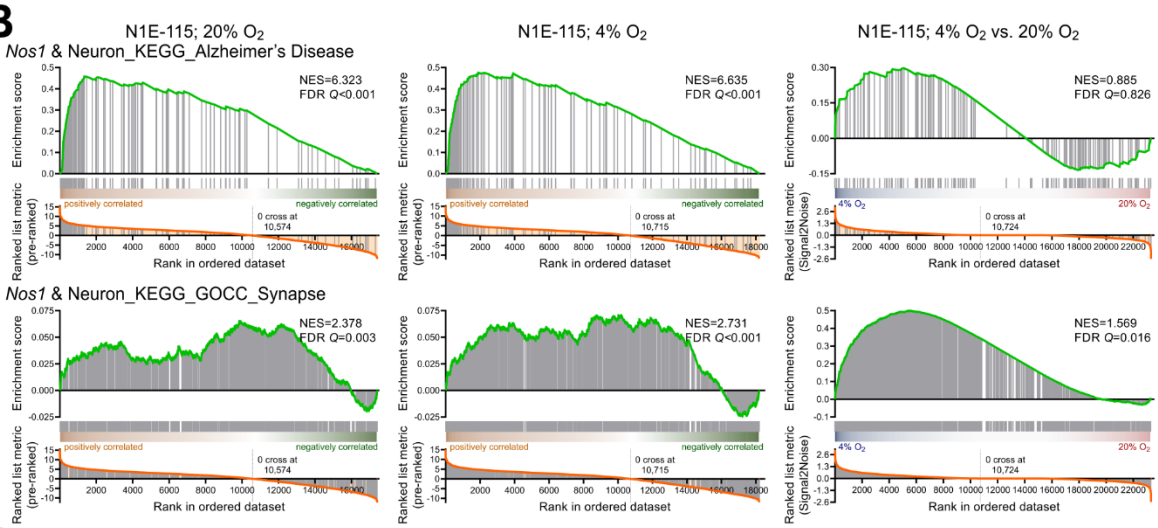

C

HALLMARK_HYPOXIA			
CONDITION	SIZE	NES	FDR Q
N1E-115; 20% O_2	186	2.907	0.000
N1E-115; 4% O_2	193	3.561	0.000
N1E-115; 4% O_2 vs. 20% O_2	207	1.907	0.001

HALLMARK_OXIDATIVE_PHOSPHORYLATION			
CONDITION	SIZE	NES	FDR Q
N1E-115; 20% O_2	198	10.061	0.000
N1E-115; 4% O_2	198	9.911	0.000
N1E-115; 4% O_2 vs. 20% O_2	200	-1.417	0.044

HALLMARK_GLYCOLYSIS			
CONDITION	SIZE	NES	FDR Q
N1E-115; 20% O_2	189	4.061	0.000
N1E-115; 4% O_2	194	4.515	0.000
N1E-115; 4% O_2 vs. 20% O_2	210	1.861	0.000

D

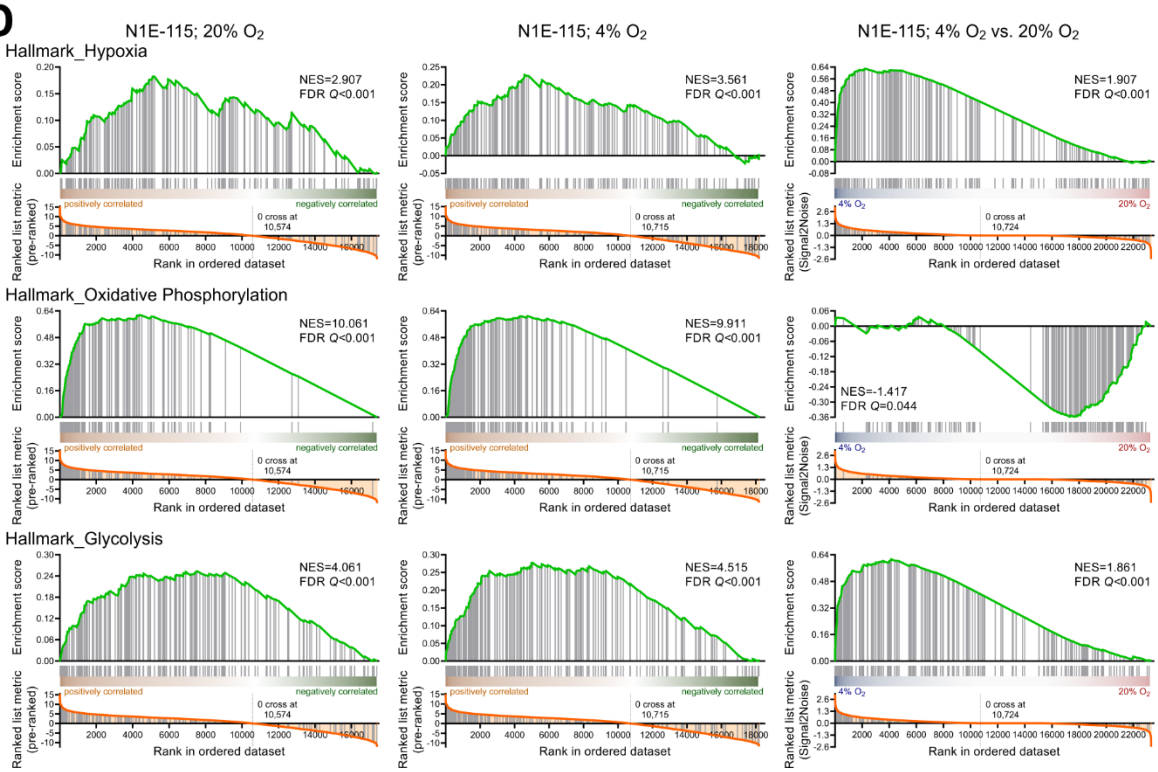

Supplementary Figure 4. *Nos1* gene expression and hypoxic signaling are active in N1E-115 cells and upregulated by environmental hypoxia. (*A*) Enrichment of *Nos1*-related gene sets from the *Nos1*&Neuron gene set matrix detected by pre-ranked (20% O_2 and 4% O_2) and standard (4% O_2 vs. 20% O_2) GSEA applied to total RNA-seq data (*n*=3/condition) in N1E-115 cells cultured for 3 days at 20% or 4% O_2. Cutoff: FDR<0.25. Right panels: heat maps of GSEA leading edge analysis results. See genes and gene sets in **Supplementary Data 5** worksheets labeled "_NOS1&NEURON_LEADING_EDGE". The region containing *Nos1* (arrowhead) is enlarged on the left side of the panel. (*B*) Pre-ranked (20% O_2 and 4% O_2) and standard (4% O_2 vs. 20% O_2) GSEA plots of Alzheimer's disease- and synapse-related gene expression from the *Nos1*&Neuron gene set matrix in N1E-115 cells. (*C*) Enrichment of hypoxia-, OXPHOS-, and glycolysis-related gene sets from the MSigDB Hallmark v.7.4 gene set matrix detected by pre-ranked (20% O_2 and 4% O_2) and standard (4% O_2 vs. 20% O_2) GSEA applied to total RNA-seq data (*n*=3/condition) in N1E-115 cells cultured for 3 days at 20% or 4% O_2. Cutoff: FDR<0.25. (*D*) Pre-ranked (20% O_2 and 4% O_2) and standard (4% O_2 vs. 20% O_2) GSEA plots of hypoxia-, OXPHOS- and glycolysis-related gene expression from the MSigDB Hallmark v.7.4 gene set matrix in N1E-115 cells.

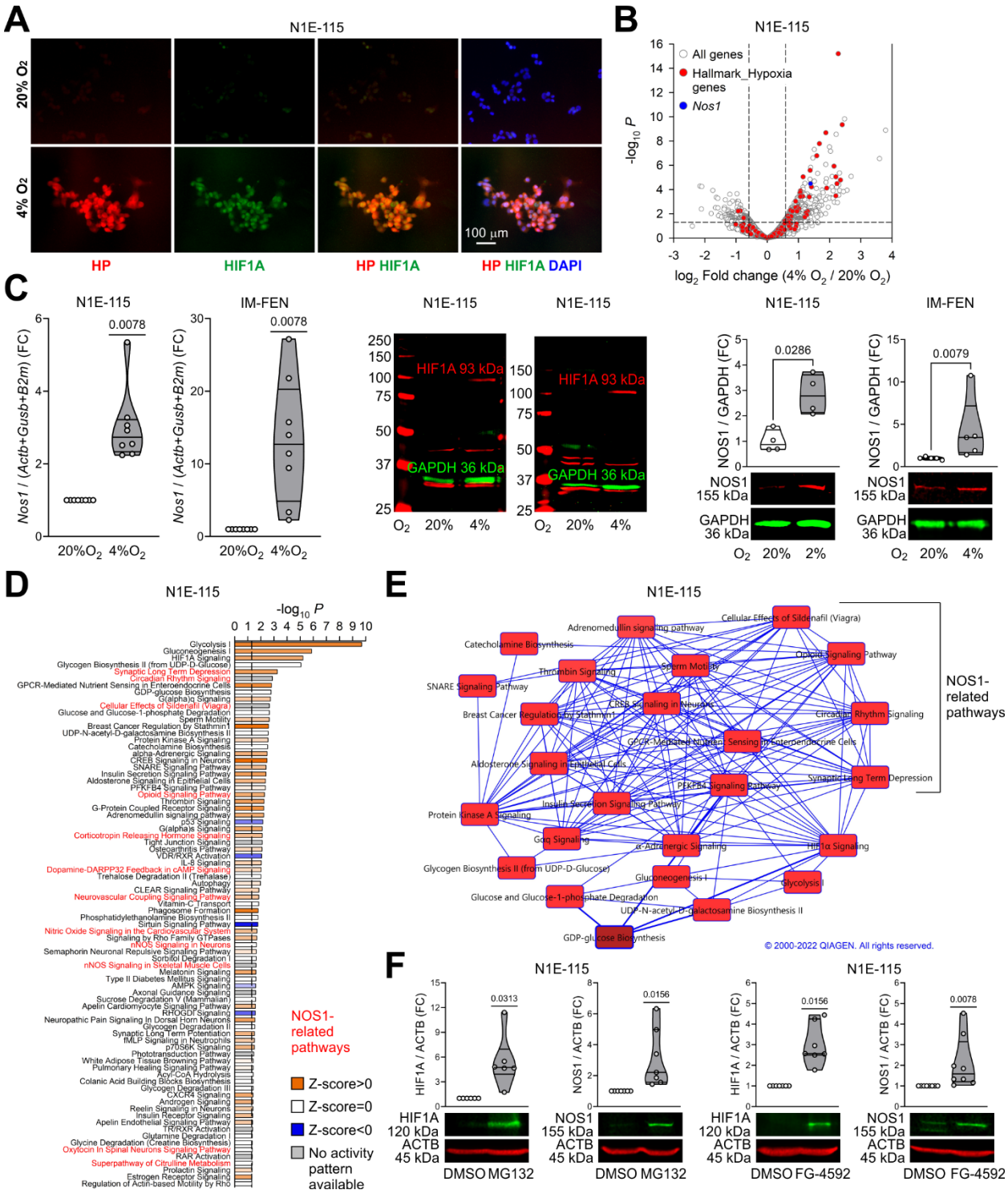

Supplementary Figure 5. Environmental hypoxia-induced or pharmacological stabilization of HIF1A increases NOS1 levels and nitrergic signaling in N1E-115 cells. (*A*) HIF1A (antibody: Cell Signaling Technology #36169) in N1E-115 cells cultured for 3 days at 4% or 20% O_2. HP, Hypoxyprobe (10 μM; 2 h). Digital overlays of pseudocolored wide-field fluorescent images (representative of 3 experiments) are shown. (*B*) Differential gene expression from total RNA-seq in N1E115 cells cultured as above (*n*=3/condition). *Nos1* and

hypoxia-related genes (MSigDB Hallmark v.7.4) are colored as indicated. (*C*) *Nos1* mRNA detected by RT-qPCR and NOS1 protein detected by immunoblotting in N1E-115 or IM-FEN cells cultured for 3 days at 4% or 2% O_2 vs. 20% O_2. Left panels: RT-qPCR; n=8/condition/cell line. Reference genes: *Actb*, *Gusb*, and *B2m*. *P* values are from Wilcoxon signed rank tests. Middle panels: HIF1A detected with Novus Biologicals NB100-134 primary antibody. Loading controls: GAPDH. Right panels: NOS1 in N1E-115 and in IM-FEN cells. Western blots were performed in 1-2 pairs of cells simultaneously and quantified relative to GAPDH detected in the same blots; $n_{\text{N1E-115}}$=4/condition; $n_{\text{IM-FEN}}$=5/condition. *P* values are from Mann-Whitney tests. (*D*) Significant (P<0.05) Ingenuity Canonical Pathways detected by IPA in the differential expression data shown in *B*. NOS1-related pathways are in red. (*E*) Ingenuity Canonical Pathways containing the same shared molecules. (*F*) Upregulation of HIF1A (Cell Signaling Technology #14179) and NOS1 protein vs. the non-HIF1A-target ACTB by HIF1A stabilization with the proteasome inhibitor MG132 (10 μM, 4 h) or the PHD inhibitor FG-4592 (20 μM, 2 days) (HIF1A: MG132 or dimethyl sulfoxide (DMSO) vehicle: n=6; FG-4592 or DMSO: n=7; NOS1: MG132 or DMSO: n=7; FG-4592 or DMSO: n=8). *P*, one sample Wilcoxon signed rank tests.

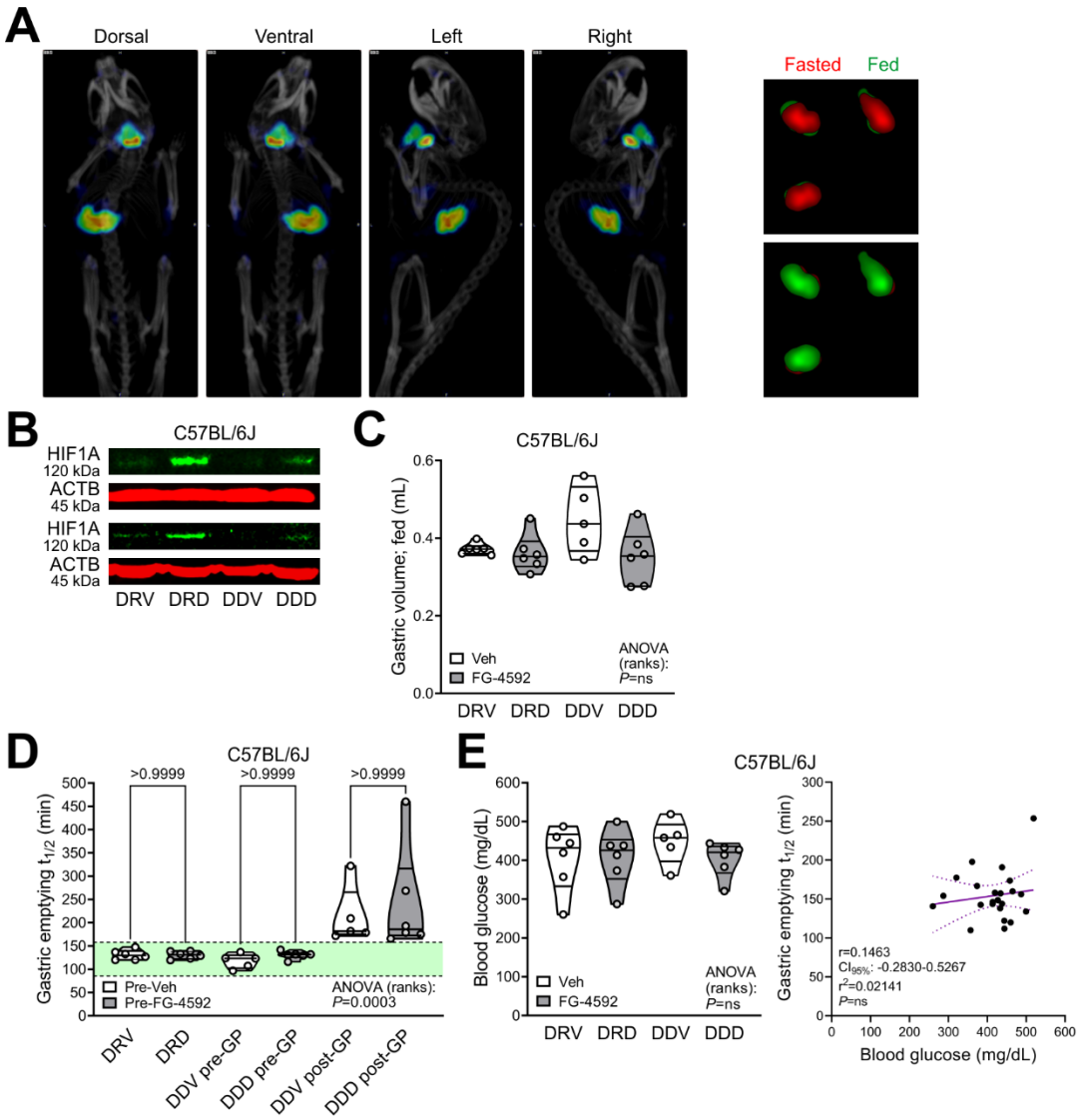

Supplementary Figure 6. Effects of in vivo HIF1A stabilization on gastric volumes, gastric emptying, and blood glucose in diabetic female C57BL/6J mice. (*A*) Visualization of the stomach by SPECT. Left: Accumulation of the ^{99m}[Tc]-pertechnetate tracer in the thyroid gland and the stomach of a representative mouse. Right: Representative segmented gastric signals in fasting and fed states. (*B*) Upregulation of HIF1A protein levels (Cell Signaling Technology #14179) in the mouse gastric corpus+antrum tunica muscularis by FG-4592 treatment. DRV, diabetic, resistant to GP, Veh-treated; DRD, diabetic, resistant to GP, FG-4592-treated; DDV, diabetic, delayed GE, Veh-treated; DDD, diabetic, delayed GE, FG-4592-treated. (*C*) Effect of FG-4592 treatment on fed GVs. *P* value is from Kruskal-Wallis ANOVA on ranks. ns, not significant. (*D*) No significant differences between pretreatment GE $t_{1/2}$ values in mice randomly assigned to FG-4592 or Veh treatment. *P* values are from Kruskal-Wallis ANOVA on ranks and Dunn's post-hoc tests. (*E*) Left panel: No effect of FG-4592 treatment on blood glucose. *P* value is from Kruskal-Wallis ANOVA on ranks. Right panel: Lack of significant correlation between blood glucose and GE $t_{1/2}$ values. $CI_{95\%}$, 95% confidence interval. *P* is from simple linear regression and Pearson correlation. ns, not significant.

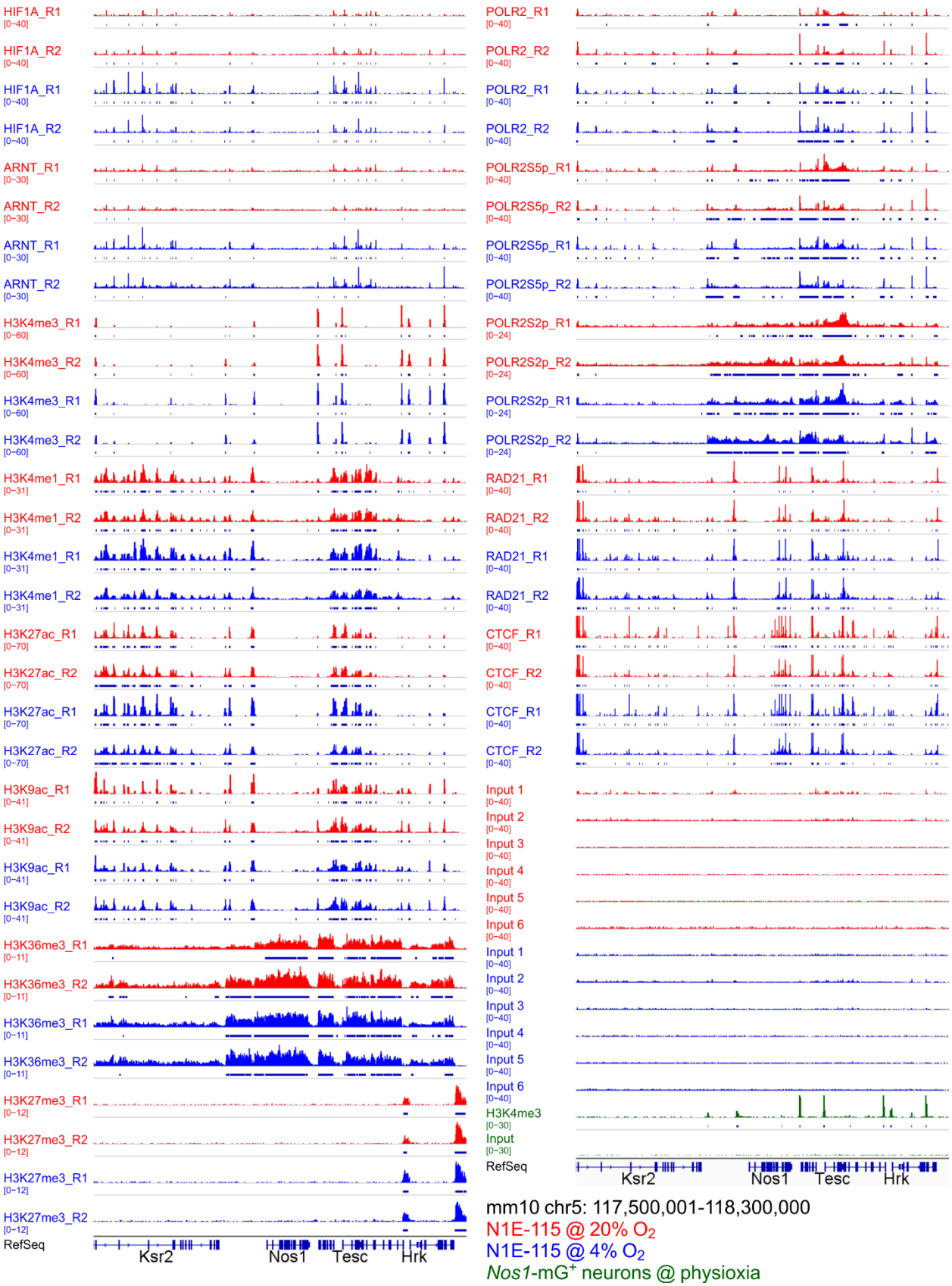
HIF1A_R1 [0–40]
HIF1A_R2 [0–40]
HIF1A_R1 [0–40]
HIF1A_R2 [0–40]
ARNT_R1 [0–30]
ARNT_R2 [0–30]
ARNT_R1 [0–30]
ARNT_R2 [0–30]
H3K4me3_R1 [0–60]
H3K4me3_R2 [0–60]
H3K4me3_R1 [0–60]
H3K4me3_R2 [0–60]
H3K4me1_R1 [0–31]
H3K4me1_R2 [0–31]
H3K4me1_R1 [0–31]
H3K4me1_R2 [0–31]
H3K27ac_R1 [0–70]
H3K27ac_R2 [0–70]
H3K27ac_R1 [0–70]
H3K27ac_R2 [0–70]
H3K9ac_R1 [0–41]
H3K9ac_R2 [0–41]
H3K9ac_R1 [0–41]
H3K9ac_R2 [0–41]
H3K36me3_R1 [0–11]
H3K36me3_R2 [0–11]
H3K36me3_R1 [0–11]
H3K36me3_R2 [0–11]
H3K27me3_R1 [0–12]
H3K27me3_R2 [0–12]
H3K27me3_R1 [0–12]
H3K27me3_R2 [0–12]
RefSeq
Ksr2
Nos1
Tesc
Hrk
POLR2_R1 [0–40]
POLR2_R2 [0–40]
POLR2_R1 [0–40]
POLR2_R2 [0–40]
POLR2S5p_R1 [0–40]
POLR2S5p_R2 [0–40]
POLR2S5p_R1 [0–40]
POLR2S5p_R2 [0–40]
POLR2S2p_R1 [0–24]
POLR2S2p_R2 [0–24]
POLR2S2p_R1 [0–24]
POLR2S2p_R2 [0–24]
RAD21_R1 [0–40]
RAD21_R2 [0–40]
RAD21_R1 [0–40]
RAD21_R2 [0–40]
CTCF_R1 [0–40]
CTCF_R2 [0–40]
CTCF_R1 [0–40]
CTCF_R2 [0–40]
Input 1 [0–40]
Input 2 [0–40]
Input 3 [0–40]
Input 4 [0–40]
Input 5 [0–40]
Input 6 [0–40]
Input 1 [0–40]
Input 2 [0–40]
Input 3 [0–40]
Input 4 [0–40]
Input 5 [0–40]
Input 6 [0–40]
H3K4me3 [0–30]
Input [0–30]
RefSeq
Ksr2
Nos1
Tesc
Hrk
mm10 chr5: 117,500,001-118,300,000
N1E-115 @ 20% O_2
N1E-115 @ 4% O_2
Nos1-mG$^+$ neurons @ physioxia

Supplementary Figure 7. Epigenetic profiling of the *Nos1* locus in mouse nitrergic neurons by ChIP-seq. Binding profiles of the indicated transcription factors, RNA polymerase II, and histone marks in the topologically associating domain containing *Nos1* (see **Figure 5*A*** and **Supplementary Figure 10*B***) in N1E-115 cells cultured at 20% O_2 (red tracks) or 4% O_2 (blue tracks) for 3 days. Individual replicates are shown. The green track represents H3K4me3 data from genetically labeled nitrergic neurons purified by FACS from the small intestines of tamoxifen-treated *Nos1*$^{creERT2/+}$;*R26*^{mTmG} mice.

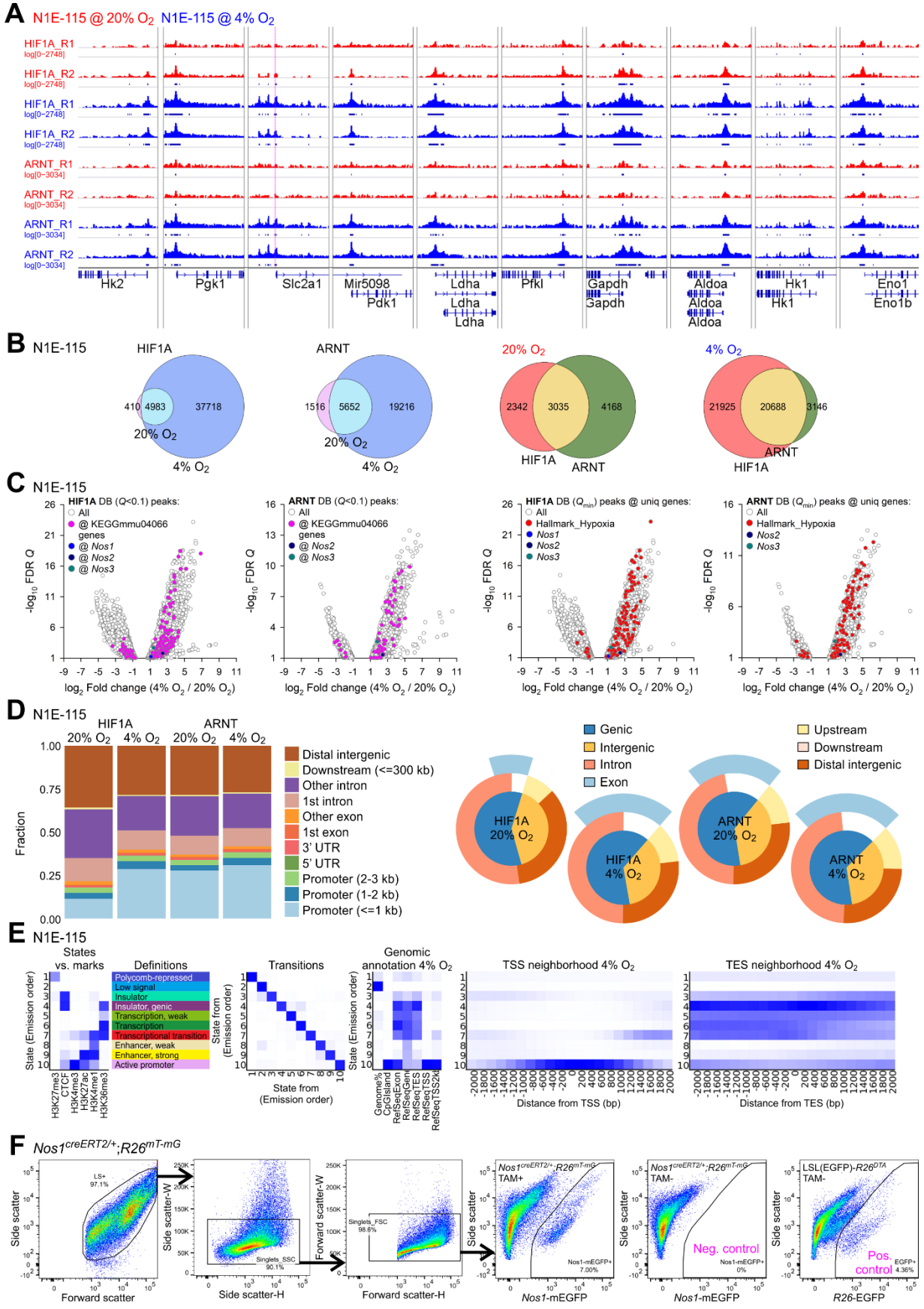
A
N1E-115 @ 20% O2
N1E-115 @ 4% O2
HIF1A_R1
HIF1A_R2
HIF1A_R1
HIF1A_R2
ARNT_R1
ARNT_R2
ARNT_R1
ARNT_R2
log[0-2748]
log[0-3034]
Hk2
Pgk1
Slc2a1
Mir5098
Pdk1
Ldha
Ldha
Ldha
Pfkl
Gapdh
Gapdh
Aldoa
Aldoa
Aldoa
Hk1
Hk1
Eno1
Eno1b
B
N1E-115
HIF1A
410
4983
37718
20% O2
4% O2
ARNT
1516
5652
19216
20% O2
4% O2
20% O2
2342
3035
4168
HIF1A
ARNT
4% O2
21925
20688
3146
ARNT
HIF1A
C
N1E-115
HIF1A DB (Q<0.1) peaks:
All
@ KEGGmmu04066 genes
@ Nos1
@ Nos2
@ Nos3
ARNT DB (Q<0.1) peaks:
All
@ KEGGmmu04066 genes
@ Nos2
@ Nos3
HIF1A DB (Qmin) peaks @ uniq genes:
All
Hallmark_Hypoxia
Nos1
Nos2
Nos3
ARNT DB (Qmin) peaks @ uniq genes:
All
Hallmark_Hypoxia
Nos2
Nos3
-log10 FDR Q
log2 Fold change (4% O2 / 20% O2)
D
N1E-115
HIF1A
ARNT
20% O2
4% O2
20% O2
4% O2
Fraction
Distal intergenic
Downstream (<=300 kb)
Other intron
1st intron
Other exon
1st exon
3' UTR
5' UTR
Promoter (2-3 kb)
Promoter (1-2 kb)
Promoter (<=1 kb)
Genic
Intergenic
Intron
Exon
Upstream
Downstream
Distal intergenic
HIF1A 20% O2
HIF1A 4% O2
ARNT 20% O2
ARNT 4% O2
E
N1E-115
States vs. marks
Definitions
Polycomb-repressed
Low signal
Insulator
Insulator, genic
Transcription, weak
Transcription
Transcriptional transition
Enhancer, weak
Enhancer, strong
Active promoter
State (Emission order)
H3K27me3
CTCF
H3K4me3
H3K27ac
H3K4me1
H3K36me3
Transitions
State from (Emission order)
Genomic annotation 4% O2
Genome%
CpGIsland
RefSeqExon
RefSeqGen
RefSeqTES
RefSeqTSS
RefSeqTSS2kb
TSS neighborhood 4% O2
Distance from TSS (bp)
TES neighborhood 4% O2
Distance from TES (bp)
F
Nos1creERT2/+;R26mT-mG
LS+
97.1%
Side scatter
Forward scatter
Singlets_SSC
90.1%
Side scatter-W
Side scatter-H
Singlets_FSC
98.6%
Forward scatter-W
Forward scatter-H
Nos1creERT2/+;R26mT-mG
TAM+
Nos1-mEGFP+
7.00%
Nos1-mEGFP
Nos1creERT2/+;R26mT-mG
TAM-
Neg. control
Nos1-mEGFP+
0%
Nos1-mEGFP
LSL(EGFP)-R26DTA
TAM-
Pos. control
EGFP+
4.36%
R26-EGFP

Supplementary Figure 8. Transcription factor and histone mark binding patterns in N1E-115 cells and nitrergic neuron sorting. (*A*) HIF1A and ARNT binding near the transcription start sites (TSSs) of canonical HIF1A targets transcriptionally upregulated in N1E-115 cells cultured at 4% O_2 (blue) vs. 20% O_2 (red) for 3 days. Aggregate data from two replicates are shown. Purple line identifies the HIF1A peak analyzed by ChIP in **Figure 7*B***. (*B*) Venn diagrams showing overlaps of HIF1A and ARNT peaks. (*C*) Differential HIF1A and ARNT binding in N1E-115 cells cultured for 3 days at 4% or 20% O_2. Log_2 fold changes for differentially bound (FDR *Q*<0.1) ChIP-seq peaks (left panels) and differentially bound ChIP-seq peaks with the lowest FDR *Q* value among peaks assigned to the same gene (right panels) are shown. *Nos1*, *Nos2*, *Nos3*, and hypoxia-related genes (KEGG mmu04066 and the MSigDB Hallmark v.7.4) are colored as indicated. (*D*) Left: Genomic distribution of HIF1A and ARNT binding in N1E115 cells. Right: Venn pies illustrating annotation overlaps. (*E*) Discovery and annotation of epigenetic states by ChromHMM (10-state model based on H3K27me3, CTCF, H3K4me3, H3K27ac, H3K4me1, and H3K36me3) in N1E-115 cells. Heat maps show the probability of observing the mark in the state, state transitions, functional enrichment of chromatin states, and their fold enrichment within ±2 kb of TSSs and transcription end sites (TESs). (*F*) Gating scheme to enrich *Nos1*-mG$^+$ neurons from the small intestines of tamoxifen-treated *Nos1*$^{creERT2/+}$*;R26*^{mTmG} mice by FACS. 3,500,000 *Nos1*-mG$^+$ neurons were sorted from 16 mice in 3 sessions and pooled for ChIP-seq.

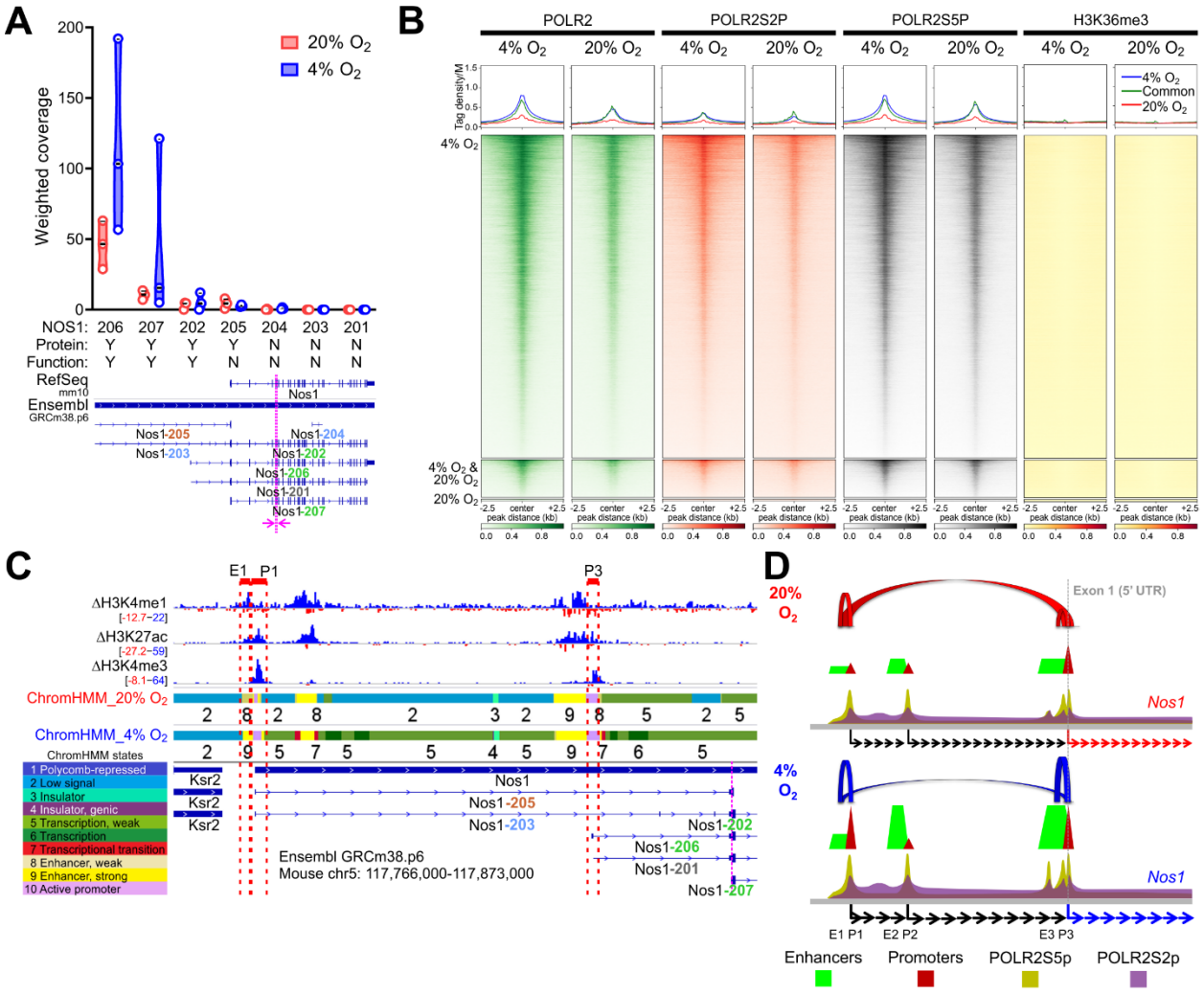

Supplementary Figure 9. HIF1A regulates Nos1 transcriptional initiation and elongation. (*A*) Expression of *Nos1* transcripts annotated in Ensembl GRCm38.p6 (ENSMUSG00000029361) and assembled from total RNA-seq data using StringTie2 in N1E-115 cells cultured at 4% or 20% O_2 for 3 days. Transcripts encoding for full-length NOS1 protein are *Nos1-206*, *Nos1-207*, and *Nos1-202* (green numbers). *Nos1-205* encodes for a truncated protein containing a PDZ domain only (orange). *Nos1-203* and *Nos1-204* are processed transcripts (light blue), and *Nos1-201* is subject to nonsense-mediated decay (gray). Parallel dashed vertical lines indicate primers used for RT-qPCR analysis. (*B*) Heat maps and average tag density plots of ChIP-seq data showing the pO_2-dependent association of HIF1A binding (see in **Figure 3*C***) with POLR2, POLR2S2p, POLR2S5p, and H3K36me3 in N1E-115 cells cultured at 20% O_2 or 4% O_2 for 3 days. Tag densities aligned to the centers of HIF1A peaks±2.5 kb are shown separately for HIF1A peaks unique to cells cultured at 4% O_2 (blue lines, top heat map panels) or 20% O_2 (red lines, bottom heat map panels) or common to cells maintained at 4% O_2 or 20% O_2 (green lines, middle heat map panels). (*C*) Positions of genomic deletions introduced into N1E-115 cells by CRISPR-Cas9 superimposed upon ΔH3K4me1, ΔH3K27ac, ΔH3K4me3, and ChromHMM tracks from **Figure 3*D***. See results in **Figure 4*B***. (*D*) Schematic diagram depicting the proposed mechanisms of HIF1A-mediated regulation of *Nos1* expression via changes in chromosome conformation and transcriptional initiation and elongation.

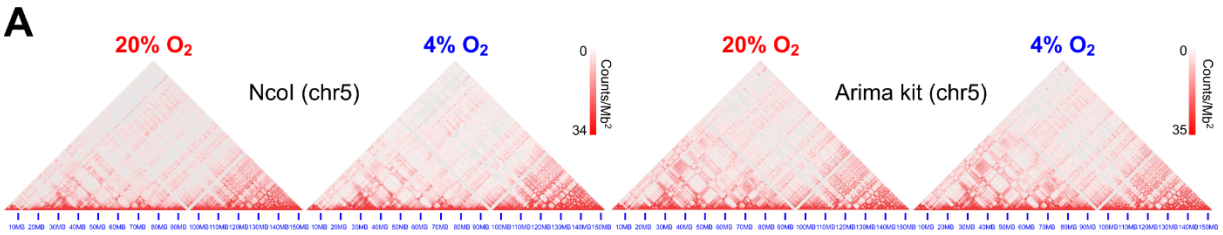

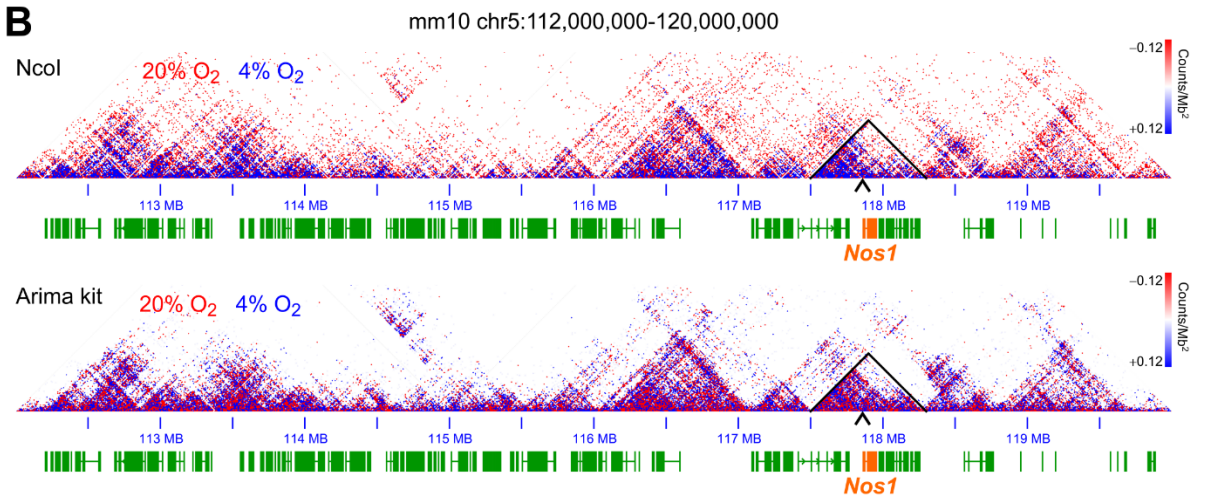

C

	HiCCUPS loops	
Size	**20% O_2**	**4% O_2**
5 kb	18879	17582
10 kb	9231	8100
25 kb	5049	4924
Total	**33159**	**30606**

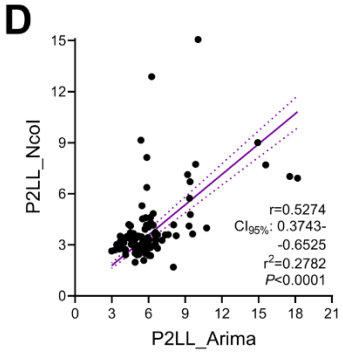

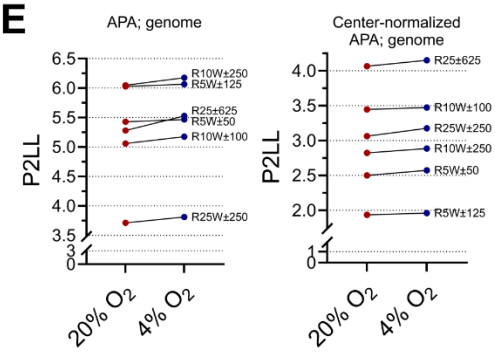

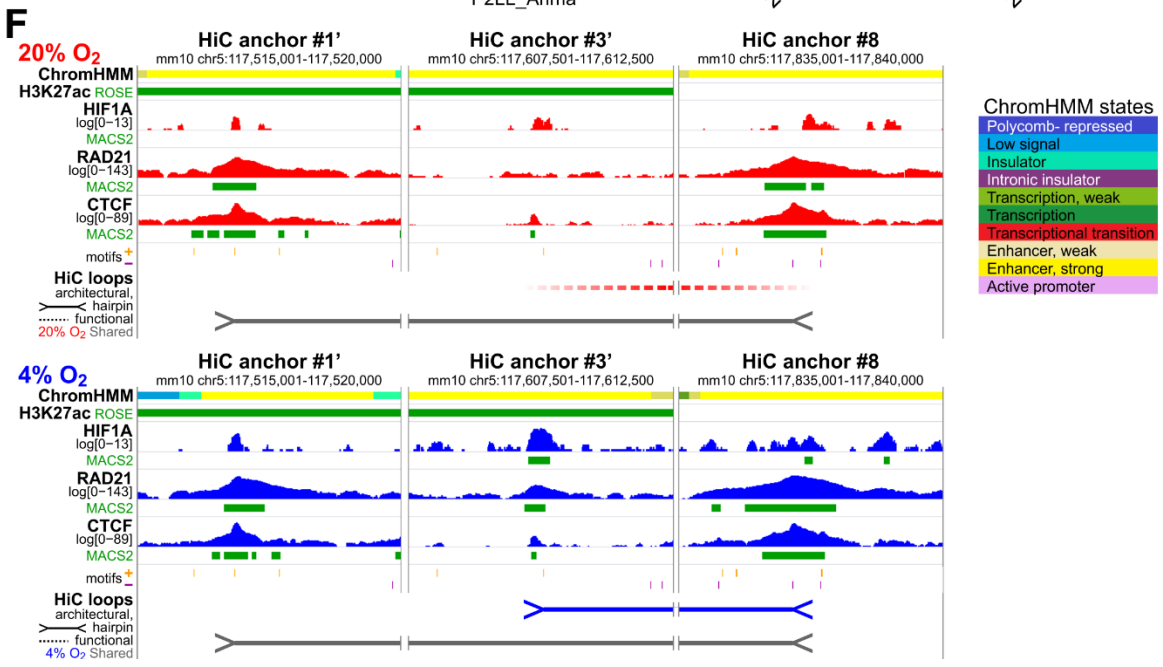

Supplementary Figure 10. HiC in N1E-115 cells. (*A*) HiC heat maps for chromosome 5 of N1E-115 cells cultured at 20% O_2 or 4% O_2 for 3 days. Chromatin was digested with *Nco*I or the Arima 2-enzyme cocktail and sequenced to generate 315-385 million read pairs/condition/experiment. (*B*) Differential HiC data (red: 20% O_2; blue: 4% O_2) from an 8-Mb region of chromosome 5 encompassing the TAD containing *Nos1* (triangles). Caret points at the *Nos1-206* TSS. (*C*) Loops detected by HiC Computational Unbiased Peak Search (HiCCUPS) at 5-, 10-, and 25-kb resolution. (*D*) Correlation of APA peak-to-lower-left (P2LL) enrichment values obtained by *Nco*I and the Arima cocktail. $CI_{95\%}$, 95% confidence interval. *P* is from linear regression and Pearson correlation. (*E*) Standard and center-normalized, genome-wide APA P2LL data obtained in N1E-115 cells cultured at 20% O_2 (red) or 4% O_2 (blue) for 3 days. P2LL values obtained at 5-, 10-, or 25-kb resolution (R) with window (W) sizes peak center±resolution×10 or ×25 are shown. (*F*) Conversion of a functional loop detected at 20% O_2 (dashed red line with fuzzy ends) into an architectural loop at 4% O_2 (solid blue line). HIF1A, RAD21, and CTCF binding at representative HiC anchors (numbered as in **Figure 5*B*** and ***C***) are shown. Note gain of significant HIF1A peaks at both anchors #3' and #8 and the gain of a RAD21 peak at anchor #3'. Solid gray lines illustrate a HIF1A-independent architectural loop significant at both 20% and 4% O_2.

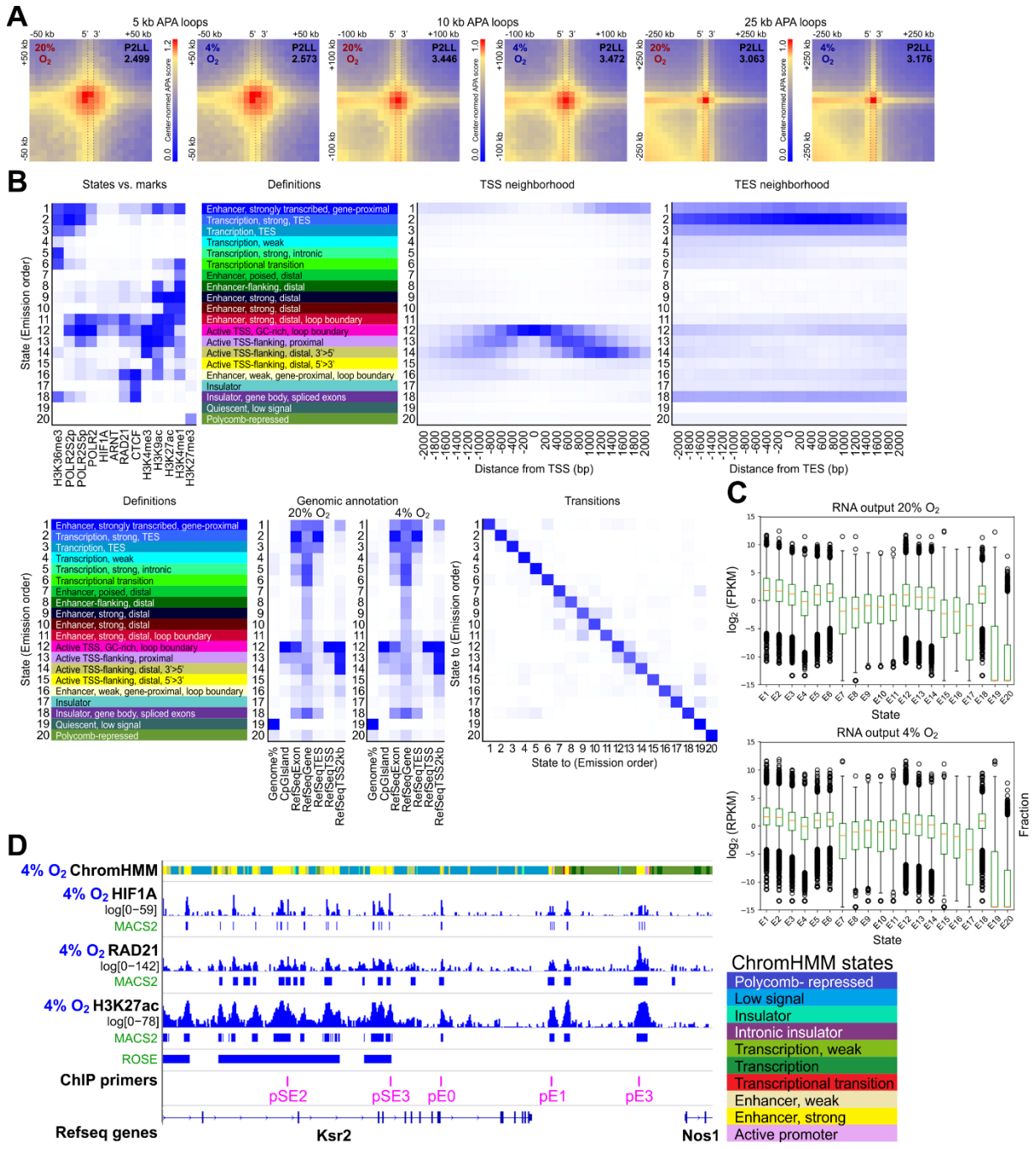

Supplementary Figure 11. HIF1A regulates chromosome topology. (*A*) Heat maps of center-normalized APA results obtained at 5-kb, 10-kb, and 25-kb resolution and analyzed over genomic distances of peak center±resolution×10 at 20% O_2 or 4% O_2. P2LL, peak-to-lower-left-quadrant enrichment values. (*B*) Discovery and annotation of epigenetic states by ChromHMM in N1E-115 cells cultured at 20% or 4% O_2 for 3 days. The 20-state model was based on the full set of ChIP-seq data (see legend to **Supplementary Figure 8*E*** for further details). (*C*) RNA output (log_2 FPKM) of each state at 20% or 4% O_2. (*D*) Key SEs and enhancers of the *Nos1* sub-TAD analyzed by ChIP-qPCR for HIF1A and RAD21 binding using primers targeting the indicated genomic loci as shown in **Figure 7*C***. The colored ribbon identifies epigenetic states discovered by ChromHMM using a 10-state model. Data obtained at 4% O_2 are shown.

Supplementary Tables

Supplementary Table 1. CrRNAs and primers for validating CRISPR-Cas9-mediated deletions

Clone	5’ cut	3’ cut	Note
E1-1	GCTATAACTTTAGACCCCCA	AGAAATTACGACCTGCTGAT	crRNA
E1-2	GGTCTAAAGTTATAGCAACT	GTTTTCCTGATCCAAACAAG	crRNA
P1-1	AATGCTCAGTTAACGCTCCC	TTTTATATGGCTAGCCGTGC	crRNA
P1-2	TTAACGCTCCCAGGATTCCT	TTTTATATGGCTAGCCGTGC	crRNA
P3-1	AAGTAGCCGCTCGCGCCCTG	ACACTCTTCATCATTGGGGG	crRNA
P3-2	CGAGCGGCTACTTAGCACAG	CACACTCTTCATCATTGGGG	crRNA
	Forward (5’-3’)	Reverse (5’-3’)	
E1	GGAGTTTCTCCTCTTCCGATTC	GATAGAGGTGGCTCAGGTTTC	PCR primers external
P1	GCAGCACAGGCACCTATC	GGGTAAATACGACCCAAATACATTG	PCR primers external
P3	GGTTGGACGTCACCACTAAT	CAAATCGAGGTGCAGGTAGTTA	PCR primers external
E1	GGAGTTTCTCCTCTTCCGATTC	CCTAAGCTAGAGCCACAGATTT	PCR primers internal
P1	GCAGCACAGGCACCTATC	TCCCTAGACTCTGACCTTTCTT	PCR primers internal
P3	GGTTGGACGTCACCACTAAT	CCTGAGAAGGTACATGGGATAC	PCR primers internal

Supplementary Table 2. Configurations of sorting cytometers used in this study

FACSAria II				FACSAria IIu			
Laser	**Detector**	**Dichroic**	**Filter**	**Laser**	**Detector**	**Dichroic**	**Filter**
				355 nm	A	595 LP	650 LP
					B	402 LP	450/50
					C	Blank	379/28
405 nm	A	750 LP	780/60	407 nm	A	750 LP	780/60
	B	690 LP	710/50		B	690 LP	710/50
	C	635 LP	670/30		C	595 LP	610/20
	D	595 LP	610/20		D	505 LP	525/50
	E	495 LP	525/50		E	Blank	450/50
	F	Blank	450/50				
488 nm	A	655 LP	670/14	488 nm	A	655 LP	670/30
	B	505 LP	525/50		B	505 LP	525/50
	C	SSC	488/10		C	SSC	488/10
	D	FSC PMT	485/22				
561 nm	A	750 LP	780/60	532 nm	A	755 LP	780/60
	B	685 LP	710/50		B	685 LP	710/50
	C	635 LP	660/20		C	640 LP	660/20
	D	595 LP	610/20		D	600 LP	610/20
	E	Blank	582/15		E	Blank	575/25
640 nm	A	750 LP	780/60	635 nm	A	755 LP	780/60
	B	685 LP	730/45		B	710 LP	730/45
	C	Blank	670/30		C	Blank	670/30

Dichroic mirror (LP, long-pass) and bandpass (center of transmittance/bandwidth) filter data are in nm. SSC, side scatter; FSC, forward scatter, PMT, photomultiplier tube.

Supplementary Table 3. Antibodies used in the immunofluorescence, Western blotting, immunoprecipitation, and chromatin immunoprecipitation studies

Target/species	Supplier	Host	Clone/ID	Isotype/lot #	Label	Final conc.	Assay
CD45 (PTPRC)/m	eBioscience	Rat mc	30-F11	IgG_{2b} κ	PE-Cy7	0.0312µg/10^6 cells	FACS
CD11b (ITGAM)/m	eBioscience	Rat mc	M1/70	IgG_{2b} κ	PE-Cy7	0.0312µg/10^6 cells	FACS
F4/80 (ADGRE1)/m	eBioscience	Rat mc	BM8	IgG_{2a} κ	PE-Cy7	0.0625µg/10^6 cells	FACS
Pimonidazole	Hypoxyprobe	Mouse mc	4.3.11.3		DyLight 549	1:200	IF
NOS1/m	SCBT	Rabbit pc	R-20; sc-648			1:200	IF
NOS1/h	SCBT	Mouse mc	A-11; sc-5302	IgG_1 κ		1 µg/mL	IF
KIT/m	DAKO	Rabbit pc	A4502	10042820A		1:200	IF
HIF1A/h	Novus	Rabbit pc	NB100-134			5 µg/mL	IF
HIF1A/h	Thermo	Rabbit mc	16H4L13; 700505	IgG		2.5 µg/mL	IF
HIF1A/m	CST	Rabbit mc	D1S7W; #36169	IgG		1:1,000	IF
TUJ1 (TUBB3)/m	CST	Rabbit pc	#5666			1:100	IF
PGP 9.5 (UCHL1)/m	Abcam	Chicken pc	ab72910	IgY		1:500	IF
HuC/D (ELAVL3/4)/m	Thermo	Mouse mc	16A11; A-21271	IgG_{2b} κ		1:100	IF
Rabbit IgG (H)	Thermo	Goat rpc	A27034	IgG	AF488	5 µg/ml	IF
Rabbit IgG (H+L)	Thermo	Goat pc	A-11008	IgG	AF488	5 µg/ml	IF
Rabbit IgG (H+L)	Thermo	Goat pc	A-21245	IgG	AF647	1:500	IF
Rabbit IgG (H+L)	Thermo	Donkey pc	A-31573	IgG	AF647	1:450	IF
Rabbit IgG (H+L)	Jackson	Donkey pc	AB_2492288; 711-605-152	IgG	AF647	3.3 µg/ml	IF
Rabbit IgG (H+L)	Jackson	Donkey pc	AB_2340616; 711-475-152	IgG	DyLight 405	1:200	IF
Chicken IgY (H+L)	Thermo	Goat pc	A-11039	IgG	AF488	5 µg/ml	IF
Chicken IgY (H+L)	Jackson	Goat pc	AB_2337389; 103-475-155	IgG	DyLight 405	1:500	IF
Chicken IgY (H+L)	Jackson	Donkey pc	AB_2340373; 703-475-155	IgG	DyLight 405	1:200	IF

Mouse IgG (H+L)	Thermo	Donkey pc	A-21202	IgG	AF488	1:450	IF
Mouse IgG (H+L)	Millipore	Donkey pc	AP192C	IgG	Cy3	2.5 µg/ml	IF
Mouse IgG (H+L)	Jackson	Donkey pc	AB_2340839; 715-475-150	IgG	DyLight 405	1:200	IF
No specific target	Jackson	Donkey pc	AB_2337258; 017-000-121	Serum		5%-10%	IF
NOS1/m	SCBT	Rabbit pc	R-20; sc-648			1:1,000	WB
HIF1A/m	CST	Rabbit mc	D2U3T; #14179	IgG		1:2,000	WB
HIF1A/m	Novus	Rabbit pc	NB100-134	IgG		1:1,000	WB
RAD21/m	CST	Rabbit pc	D213; #4321	IgG		1:2,000	WB
ACTB/m	LI-COR	Mouse mc	926-42210	IgG_{2b}		1:10,000	WB
GAPDH/m	Imgenex	Mouse mc	GAPDH 1D4; AB_316884; IMG-5019A-1			1:10,000	WB
Rabbit IgG (H+L)	LI-COR	Donkey pc	#926-32223		IRDye 680	1:10,000	WB
Mouse IgG (H+L)	LI-COR	Donkey pc	#926-32222		IRDye 680	1:10,000	WB
Rabbit IgG (H+L)	LI-COR	Donkey pc	AB_621848; #926-32213		IRDye 800CW	1:10,000	WB
Goat IgG (H+L)	LI-COR	Donkey pc	AB_621846; #926-32214		IRDye 800CW	1:10,000	WB
RAD21/m	Abcam	Rabbit pc	ab992	GR3310168-2		10µg/10^7 cells	IP
HIF1A/m	Novus	Rabbit pc	NB100-449	IgG; A6		10µg/10^7 cells	IP
No specific target	SCBT	Normal rabbit	sc-2027	IgG; E1512		10µg/10^7 cells	IP
RAD21/m	Abcam	Rabbit pc	ab992	GR3310168-2		1:2,000	WB
CTCF/m	CST	Rabbit pc	#2899	2		1:1,000	WB
Rabbit IgG (H+L)	CST	Goat pc	#7074	28	HRP	1:10,000	WB
HIF1A/m	Novus	Rabbit pc	NB100-134	IgG		2µg/10^7 cells	ChIP
ARNT/m	Novus	Rabbit pc	NB100-110	IgG		2µg/10^7 cells	ChIP
CTCF/m	CST	Rabbit pc	#2899	IgG		2µg/10^7 cells	ChIP
RAD21/m	Abcam	Rabbit pc	ab992	IgG		2µg/10^7 cells	ChIP

POLR2/m	Bethyl Labs	Rabbit pc	A300-653A	IgG		2µg/10^7 cells	ChIP
POLR2S5P/m	Active Motif	Rabbit pc	39749	IgG		2µg/10^7 cells	ChIP
POLR2S2P/m,h	Bethyl Labs	Rabbit pc	A300-654A	IgG		2µg/10^7 cells	ChIP
H3K9ac	EDL	Rabbit pc	EDL Lot2	IgG		2µg/4 x 10^6 cells	ChIP
H3K27ac	Active Motif	Rabbit pc	39133	IgG		2µg/4 x 10^6 cells	ChIP
H3K4me1	Abcam	Rabbit pc	ab8895	IgG		2µg/4 x 10^6 cells	ChIP
H3K4me3	EDL	Rabbit pc	EDL Lot1	IgG		2µg/4 x 10^6 cells	ChIP
H3K27me3	CST	Rabbit mc	C36B11; #9733	IgG		2µg/4 x 10^6 cells	ChIP
H3K36me3	Active Motif	Rabbit pc	61101	IgG		2µg/4 x 10^6 cells	ChIP

Abbreviations: Targets: m, mouse; h, human; POLR2, RNA polymerase II carboxy-terminal repeat domain YSPTSPS; POLR2S2p: RNA polymerase II carboxy-terminal repeat domain YSPTSPS phospho-S2; POLR2S5p: RNA polymerase II carboxy-terminal repeat domain YSPTSPS phospho-S5. Suppliers: eBioscience, eBioscience, Inc., San Diego, CA; Hypoxyprobe, Hypoxyprobe, Inc., Burlington, MA; SCBT, Santa Cruz Biotechnology, Inc., Dallas, TX; DAKO, DAKO North America, Inc., Carpinteria, CA; Novus, Novus Biologicals, Littleton, CO; Thermo, Thermo Fisher Scientific, Waltham, MA; CST, Cell Signaling Technology, Inc., Beverly, MA,USA; Abcam, Abcam, Inc., Cambridge, MA; Jackson, Jackson ImmunoResearch Laboratories, Inc., West Grove, PA; Millipore, EMD Millipore Corporation, Temecula, CA; LI-COR, LI-COR Biosciences, Lincoln, NE; Imgenex, Imgenex Corp., San Diego, CA; Active Motif, Active Motif, Inc., Carlsbad, CA; Bethyl Laboratories, Inc., Montgometry, TX, EDL, Epigenomics Development Laboratory, Mayo Clinic Center for Individualized Medicine, Rochester, MN. Host: mc, monoclonal; pc, polyclonal; rpc, recombinant polyclonal. Labels: PE, phycoerythrin; Cy, cyanine; AF, Alexa Fluor; HRP, horseradish peroxidase. Assay: FACS, fluorescence-activated cell sorting; IF, immunofluorescence; WB, Western blot; Co-IP: co-immunoprecipitation; ChIP, chromatin immunoprecipitation.

Supplementary Table 4. Primers for real-time reverse transcription—polymerase chain reaction (RT-qPCR)

Gene (mouse)	Forward (5'-3')	Reverse (5'-3')
Nos1	GTCCGCACCAAGGACCAGCTC	ACACAGCGAGAGGCGTTCCG
Actb	ATGGTGGGAATGGGTCAGAAG	GCTCATTGTAGAAGGTGTGGTGCC
Gusb	AGGGTTTCGAGCAGCAATGG	ATCCCATTCACCCACACAACTG
B2m	TCTCACTGACCGGCCTGTATGCTAT	TCCTTGCTGAAGGACATATCTGACATC

Supplementary Table 5. Primers for targeted ChIP of RAD21 in siHIF1A N1E115 cells.

Position	Forward (5'-3')	Reverse (5'-3')
Slc2a1	ACAGAACCACGCCTCTCAG	CATTGGTTCTGGGGTGTAGG
SE2	GCTTTCAGTCTCTGGCAAGG	CCCTTCCCTCTCCTCTCTTC
SE3	GCCGGATGTCAGCACTATTC	GACAACCAAAAGCCAGGAAA
E0	GCACACAGTCTCCAGCTCAG	GAGGGTGCATGGAAAGTACC
E1	GGCCACCTGGTGTCAATTA	CTCCCCATCTGGAGAGACTG
E3	GCCAGATTGCTCCGATAAAC	TGCCACAGTTCCTGAAGATG

Supplementary Table 6. Probes and primers for 3C

	Sequences
Probe P3	CTGGGCCCAGGCTGCAAGGACT
Primer P3 Forward	ACTCCCACAAGGACCAGCTA
Probe P1+E1	ACAGCCTGCCTCTGGTGTTCATCCTTCA
Primer P1+E1 Forward	TAAGGCAGGTCTGGAAAGCT
Primer E1 Reverse	ATGGCTGAAGGATGAACACC
Primer E1-2 Reverse	TCAGGCCCAAGTCCTAATTG
Primer E1-3 Reverse	GCTTAGGGAGCAAGCATAGC
Primer E2 Reverse	ATGTGGAAGACCACGGCTAT
Primer E2-2 Reverse	CTAGCCAGATGTGGGTGGAG
Primer CTCF Reverse	TTCTGCTTCCTGGCACCTAT
Primer CTCF 2 Reverse	ACATTGATTTCTGCCCTCCA
Primer E 3 Reverse	GGAATCGATGCAGAGACCAT
Primer E3-2 Reverse	ATGACACCCCTCCCTTATCC
Primer E3-3 Reverse	GGAGTTGCAGGACTCAGGTC
Primer E3-4 Reverse	GGAGCTCACTCGGGTACATC
Primer control 1 Reverse	AACCAAGGCATAGACCTGGA
Primer control 2 Reverse	CTCATACCACGCTCCCTCAT

Supplementary Videos

Supplementary Video 1. Three-dimensional rendering of an overnight fasted mouse injected with 0.3 mCi ^{99m}Tc and imaged by SPECT under isoflurane inhalation anesthesia (2%). Note accumulation of the tracer in the stomach and the thyroid gland.

Supplementary Video 2. Three-dimensional rendering of a stomach of a ^{99m}Tc-injected mouse imaged by SPECT after overnight fasting (red) and immediately following the consumption of 100 µL Ensure (green). Both images were taken under isoflurane inhalation anesthesia (2%). Note increased proximal gastric volume in the fed state.

Supplementary Data

Supplementary Data 1. Affymetrix Mouse Genome 430.2 microarray data generated from colonic *Mapt*-EGFP$^+$ neurons. Expression values and Present/Missing/Absent (PMA) calls are shown. Gene symbols are from annotation na36.

Supplementary Data 2. Gene sets and genes in the *Nos1*&Neuron gene set collection.

Supplementary Data 3. Gene Set Enrichment Analysis results for *Mapt*-EGFP$^+$ colonic neurons, *Phox2b*-CFP$^+$ duodenal, ileal, and colonic neurons, and *Baf53b*-Tom$^+$ colonic neurons. Worksheets labeled "_RPT" show analysis parameters. Other worksheets show the gene set enrichment results for the *Nos1*&Neuron and MSigDB Hallmark matrices, detailed enrichment metrics for selected gene sets, and leading-edge results for the *Nos1*&Neuron matrix.

Supplementary Data 4. Total RNA-seq results in N1E-115 cells cultured for 3 days at 20% or 4% O_2.

Supplementary Data 5. Gene Set Enrichment Analysis of RNA-seq data obtained in N1E-115 cells cultured for 3 days at 20% or 4% O_2 and of the genes that were differentially expressed at 4% vs 20% O_2. Worksheets labeled "_RPT" show analysis parameters. Other worksheets show the gene set enrichment results for the *Nos1*&Neuron and MSigDB Hallmark matrices, detailed enrichment metrics for selected gene sets, and leading-edge results for the *Nos1*&Neuron matrix.

Supplementary Data 6. QIAGEN Ingenuity Pathway Analysis of the differentially expressed genes in N1E-115 cells cultured for 3 days at 4% or 20% O_2.

Supplementary Data 7. Library complexity, mapping, and peak calling results of the chromatin immunoprecipitation-sequencing experiments.

Supplementary Data 8. Differential binding analysis results for HIF1A and ARNT in N1E-115 cells cultured for 3 days at 4% O_2 vs 20% O_2.

Supplementary Data 9. Analysis of transcription factor binding motifs (HOMER, known motifs) within the genomic footprints of the HIF1A and ARNT peaks in the vicinity of the Kyoto Encyclopedia of Genes and Genomes mmu04066 genes.

Supplementary Data 10. Chromosome loops detected by HiC Computational Unbiased Peak Search in N1E-115 cells cultured at 4% or 20% O_2.

Supplementary Data 11. Anchor sites of chromosome loops detected by Arima HiC within the topologically associating domain containing *Nos1* in N1E-115 cells cultured at 4% or 20% O_2.

Supplementary Data 12. Analysis of transcription factor binding motifs (HOMER, known motifs) in HIF1A-bound *cis*-regulatory elements of the *Nos1* topologically associating domain in N1E-115 cells.

Full-size Wide-field Fluorescent Images

Figure 1*B*

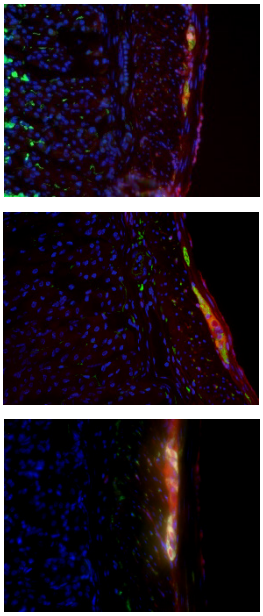

Figure 1*E*, top

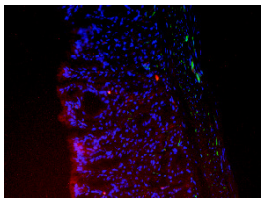

Supplementary Figure 2*A*

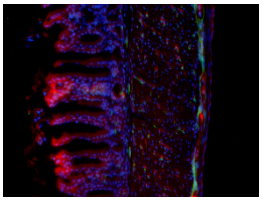

Figure 2*A*

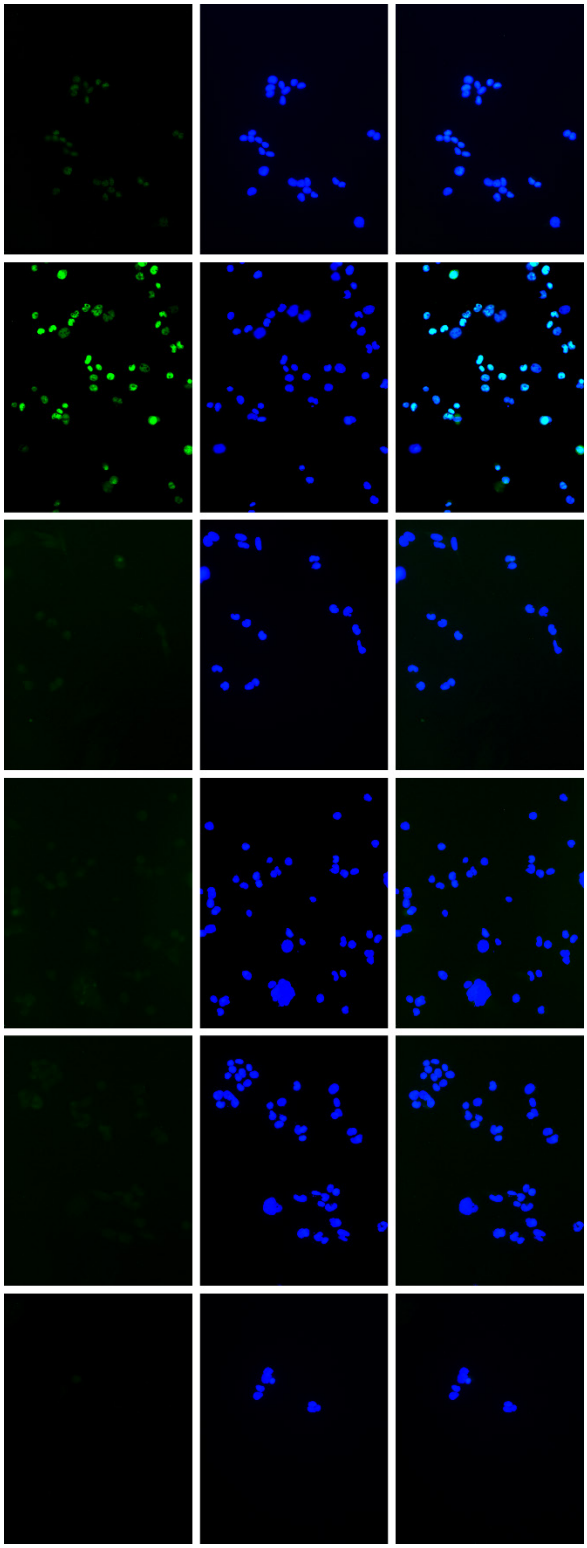

Full-size Western Blots

Figure 1*D*

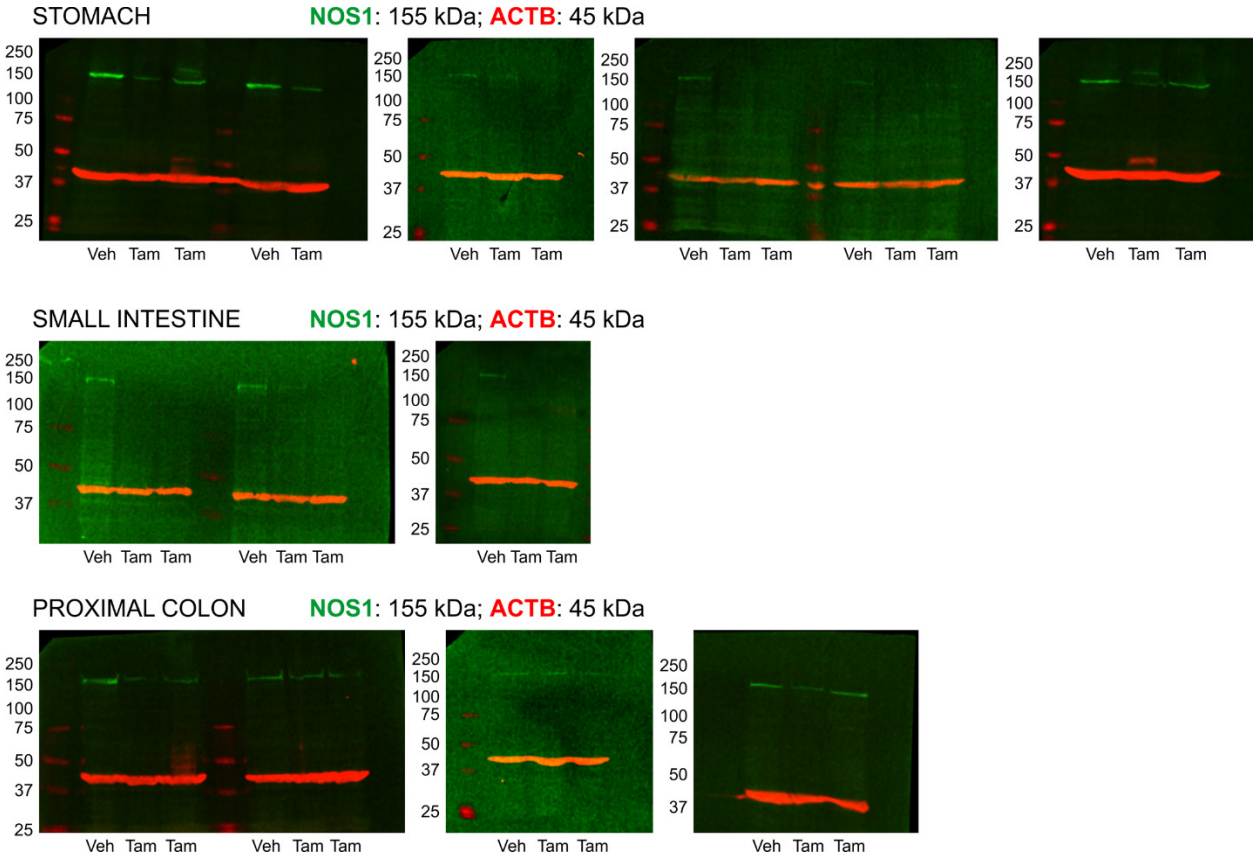

Figure 2*A*

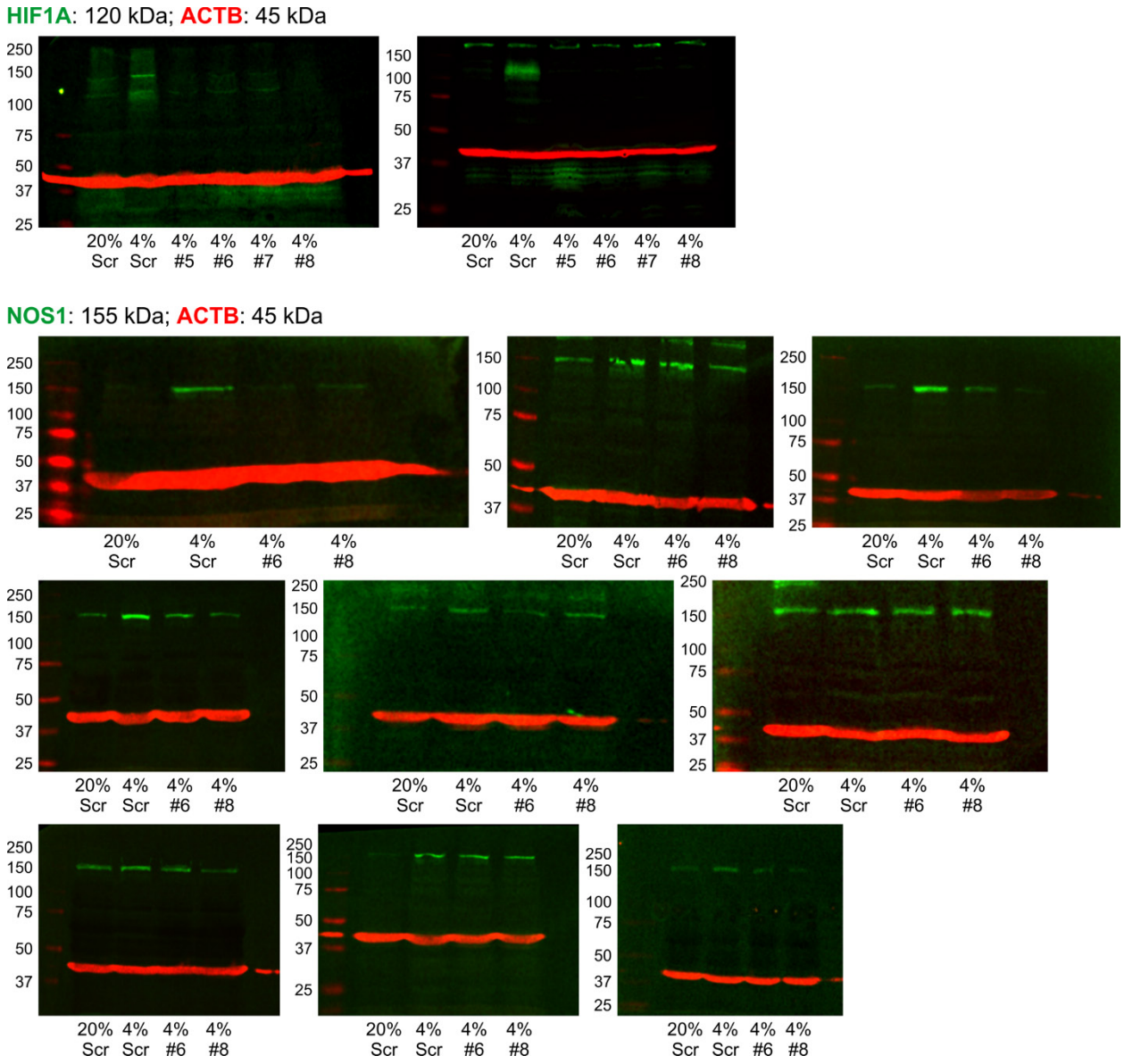
HIF1A: 120 kDa; ACTB: 45 kDa
250
150
100
75
50
37
25
20% Scr
4% Scr
4% #5
4% #6
4% #7
4% #8
NOS1: 155 kDa; ACTB: 45 kDa
20% Scr
4% Scr
4% #6
4% #8

Figure 2*B*

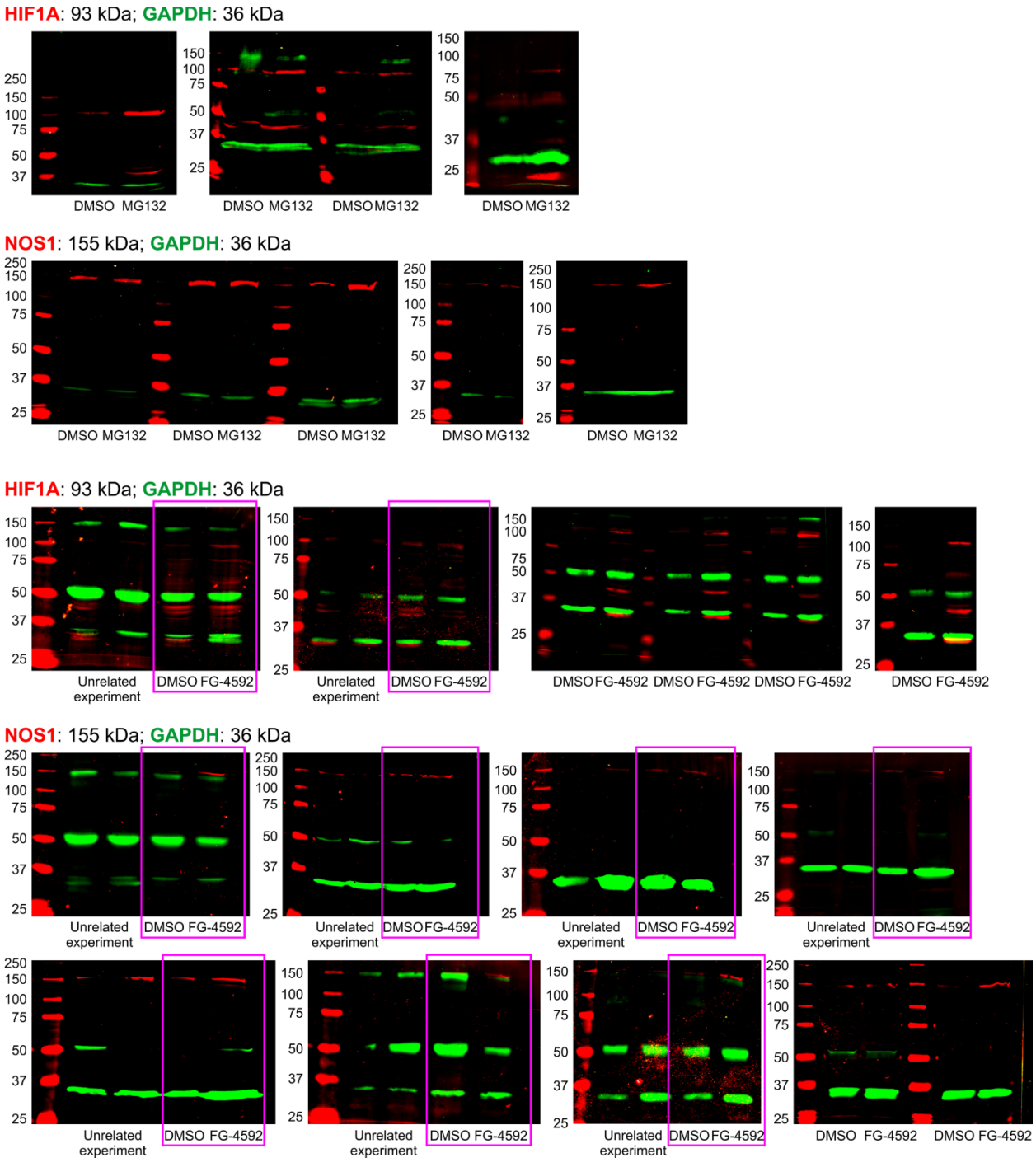
HIF1A: 93 kDa; GAPDH: 36 kDa
DMSO MG132
DMSO MG132 DMSO MG132
DMSO MG132
NOS1: 155 kDa; GAPDH: 36 kDa
DMSO MG132 DMSO MG132 DMSO MG132
DMSO MG132
DMSO MG132
HIF1A: 93 kDa; GAPDH: 36 kDa
Unrelated experiment
DMSO FG-4592
Unrelated experiment
DMSO FG-4592
DMSO FG-4592 DMSO FG-4592 DMSO FG-4592
DMSO FG-4592
NOS1: 155 kDa; GAPDH: 36 kDa
Unrelated experiment
DMSO FG-4592
Unrelated experiment
DMSO FG-4592
Unrelated experiment
DMSO FG-4592
Unrelated experiment
DMSO FG-4592
Unrelated experiment
DMSO FG-4592
Unrelated experiment
DMSO FG-4592
Unrelated experiment
DMSO FG-4592
DMSO FG-4592
DMSO FG-4592

Figure 2*D*

NOS1: 155 kDa; **ACTB**: 45 kDa

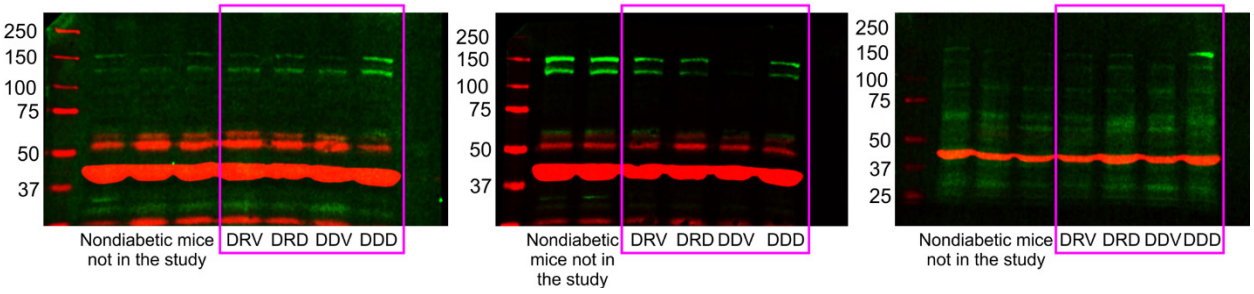

Figure 7*B*

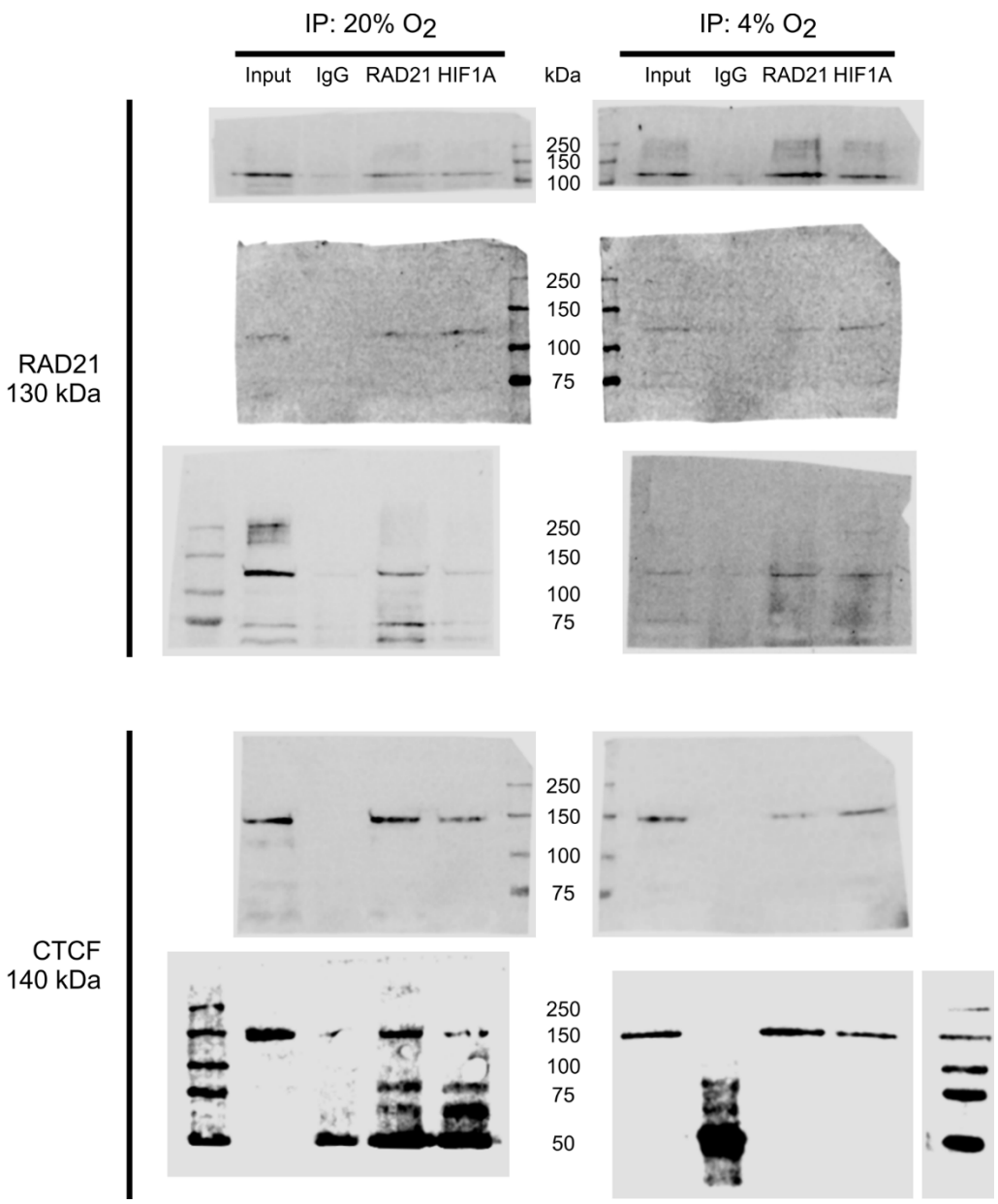
IP: 20% O2
IP: 4% O2
Input
IgG
RAD21
HIF1A
kDa
250
150
100
75
50
RAD21
130 kDa
CTCF
140 kDa

Figure 7*D*

TOP PANEL **RAD21**: 130 kDa; **ACTB**: 45 kDa

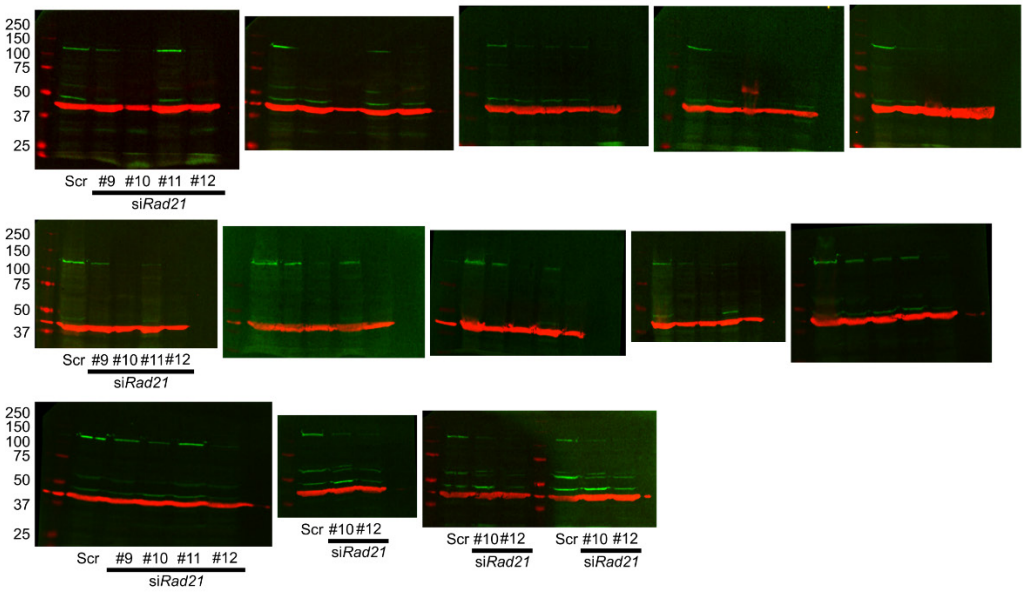

BOTTOM PANEL **NOS1**: 155 kDa; **ACTB**: 45 kDa

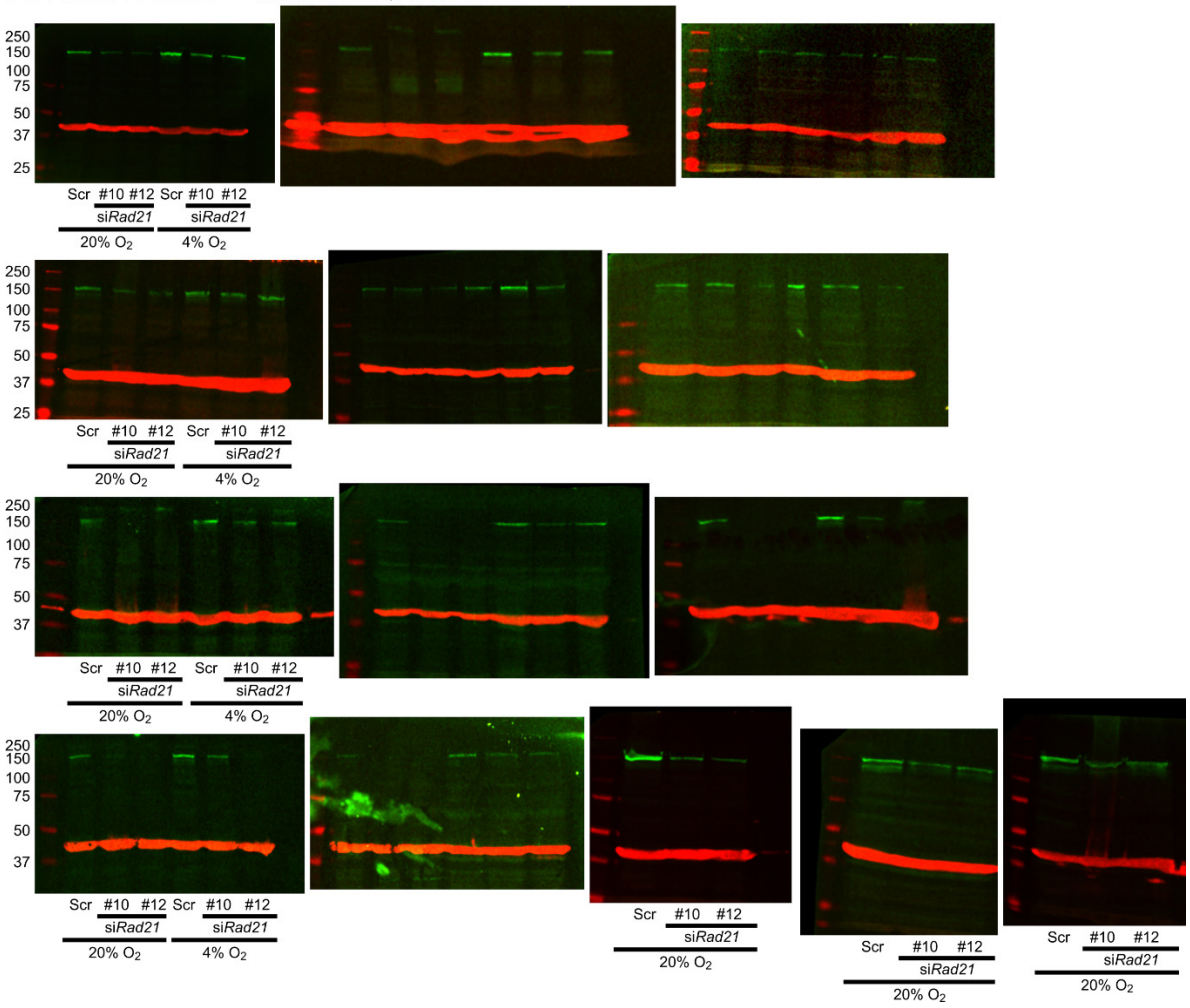

Supplementary Figure 5*C*

N1E-115

NOS1: 155 kDa; **GAPDH**: 36 kDa

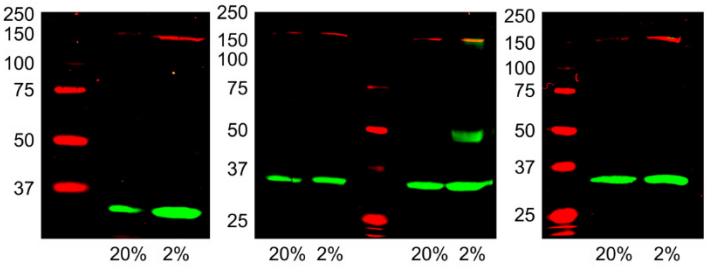

IM-FEN

NOS1: 155 kDa; **GAPDH**: 36 kDa

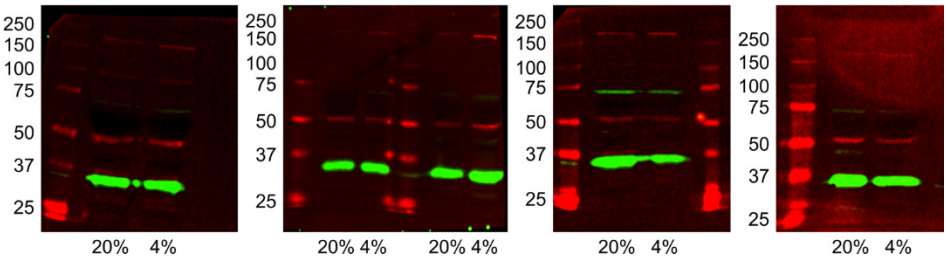

Supplementary Figure 6*B*

HIF1A: 120 kDa; **ACTB**: 45 kDa